Regional modeling of dust mass balance and radiative forcing over East Asia using WRF-Chem

Siyu Chen [a,b], Chun Zhao [b,*], Yun Qian [b], L. Ruby Leung [b], Jianping Huang [a], Zhongwei Huang [a], Jianrong Bi [a], Wu Zhang [a], Jinsen Shi [a], Lei Yang [c], Deshuai Li [d], Jinxin Li [d]

[a] Key Laboratory for Semi-Arid Climate Change of the Ministry of Education, Lanzhou University, China
[b] Atmospheric Science and Global Change Division, Pacific Northwest National Laboratory, Richland, WA, USA
[c] Nanjing University of Information Science and Technology, Nanjing, China
[d] Key Laboratory of Arid Climatic Change and Reducing Disaster of Gansu Province, Lanzhou University, China

ARTICLE INFO

ABSTRACT

The Weather Research and Forecasting model with Chemistry (WRF-Chem) is used to investigate the seasonal and inter-annual variations of mineral dust over East Asia during 2007–2011, with a focus on the dust mass balance and its direct radiative forcing. A variety of in situ measurements and satellite observations have been used to evaluate the simulation results. Generally, WRF-Chem reasonably reproduces not only the column variability but also the vertical profile and size distribution of mineral dust over and near the dust source regions. In addition, the dust lifecycle and processes that control the seasonal and spatial variations of dust mass balance are investigated over seven sub-regions of desert dust sources (Taklimakan Desert (TD) and Gobi Desert (GD)), the Tibetan Plateau (TP), Northern China, Southern China, the ocean outflow region, and Korea–Japan. Over the two major dust source regions of East Asia (TD and GD), transport and dry deposition are the two dominant sinks with contributing of ∼25% and ∼36%, respectively. Dust direct radiative forcing in a surface cooling of up to −14 and −10 W m^{-2}, atmospheric warming of up to 9 and 2 W m^{-2}, and TOA (Top of atmospheric) cooling of −5 and −8 W m^{-2}, respectively. Dust transported from the TD is the dominant dust source over the TP with a peak in summer. Over the identified outflow regions (the ocean outflow region, and Korea–Japan), maximum dust column concentration in spring is contributed by transport. Dry and wet depositions are comparable dominant sinks, but wet deposition is larger than dry deposition over the Korea–Japan region, particularly in spring (70% versus 30%). The ability of WRF-Chem to capture the measured features of dust optical and radiative properties and dust mass balance over East Asian provides confidence for future investigation of East Asia dust impact on regional or global climate.

© 2014 Elsevier B.V. All rights reserved.

1. Introduction

Dust can modulate the radiation budget (Sokolik et al., 2001; Balkanski et al., 2007; Zhao et al., 2010, 2011, 2012), affect the microphysical properties of clouds (DeMott et al., 2010; Creamean et al., 2013), alter the surface albedo of the ground covered by snow or glacier (Krinner et al., 2006; Painter et al., 2010, 2012; Huang et al., 2011; Skiles et al., 2012), and influence ocean CO_2 uptake and nutrients (Mahowald et al., 2009). In addition, dust is also important for air quality through its impact on visibility and human health (Kim et al., 2001; Chen et al., 2004; Thomson et al., 2006).

East Asia is one of the most prominent regions of dust generation (Rea, 1994; Zhang et al., 2003). Annually, a large amount of desert dust over East Asia is injected into the atmosphere of which 30% is re-deposited onto the deserts of origin, 20% is transported over continental China, and the remaining 50% falls out over the Pacific Ocean and beyond (Zhang et al., 1997). East Asian dust can significantly affect climate and ecosystems at both regional and global scales (e.g., Huang et al., 2006a,b, 2009; Qian et al., 2011). Recently, great progress has been made for East Asia dust focusing on the dust optical properties (Ge et al., 2010a,b, 2011; Liu et al., 2011), spatial and temporal characteristics (Wang et al., 2008), long-range transport (Huang et al., 2008a; Liu et al., 2008), and direct and indirect radiative forcing (Huang et al., 2009) based on satellite retrievals combined with in situ measurements.

To understand better the detailed processes affecting dust life cycle and climatic impact over East Asia, models were used to investigate East Asia dust emission, deposition, transport mechanism, and dust–climate interaction in the last decade (e.g., Zhang

et al., 2003, 2009; Gong et al., 2003; Shao and Wang, 2003; Uno et al., 2009; Sun et al., 2012; Wang et al., 2012; Chen et al., 2013). They reproduced some important observational facts to elucidate characteristics of dust phenomena and improved our understanding of dust processes over East Asia. However, few of them investigated inter- and intra-annual variation of long-term simulated East Asian dust. In addition, dust budget analysis (i.e., dust mass contributions from emission, deposition, and transport) is not well examined. Furthermore, few of previous studies investigated the dust climatic impact. Some of them intended to explore the dust climatic impact, however, the models that were used missed some important aspects, such as dust-anthropogenic aerosol interaction and dust impact on cloud properties (Zhang et al., 2009; Sun et al., 2012). In order to fully investigate the dust climatic impact, a state-of-art model that simulates dust lifecycle and dust direct and indirect feedback to climate should be used and evaluated. Not only simulated dust mass concentration but also dust size distribution, optical properties, and vertical distribution should be evaluated against observations in order to estimate robustly dust climatic impact.

For this purpose, we use the WRF-Chem model, a state-of-art model with the capability to simulate the dust direct and indirect feedbacks to climate. The WRF-Chem model is a version of the Weather Research and Forecast model (WRF) that simulates trace gases and particulates with the meteorological fields, which considers a variety of coupled physical and chemical processes such as transport, deposition, emission, chemical transformation, and radiation (Grell et al., 2005). It has the advantage in modeling dust impact on climate due to its online coupling of chemistry and meteorology. It has been widely used to simulate the dust life cycle and climatic impact at the global scale (Zhao et al., 2013a) and the regional scale over West Africa (Zhao et al., 2010, 2011), Saudi Arabia (Kalenderski et al., 2013), North America (Zhao et al., 2012), and East Asia (Chen et al., 2013). However, the dust modeling over East Asia using the WRF-Chem model has not been well evaluated yet. Therefore, in this study, various measurements of dust properties from in situ observations and satellite retrievals, including continuous measurements from the Semi-Arid Climate Observatory and Laboratory (SACOL) (Huang et al., 2008b), are used to evaluate the simulation.

In this study, the WRF-Chem model is configured with a relatively high horizontal resolution (36 km) to conduct a five-year dust simulation over East Asia from 2007 to 2011. Compared to previous works, the simulation in this study can represent better the complex topography over East Asia. The intra- and inter-annual variability of East Asian dust can also be investigated. Budget analysis is also applied during the simulation to estimate the contributions of physics- and chemistry-processes to dust life cycle, which can help us understand better the sources and sinks of East Asian dust. In addition, as a first step of investigating dust climatic impact over East Asia, this study is the first time to evaluate the performance of WRF-Chem model in simulating the temporal and spatial variability of dust over East Asia. The three major objectives of this study are to (1) evaluate the WRF-Chem simulation of dust over East Asia, (2) characterize the spatial and temporal variations of East Asian dust and its direct radiative forcing, and (3) quantify the contributions of various model processes to dust mass balance over East Asia.

2. Model description

The WRF-Chem model (v3.3.1), a version of the Weather Research and Forecasting (WRF) model (Skamarock et al., 2008), which simulates trace gases and particulates simultaneously with

the meteorological fields (Grell et al., 2005) is used in this study. The RADM2 chemical mechanism and MADE/SORGAM (Modal Aerosol Dynamics Model for Europe (MADE) and Secondary Organic Aerosol Model (SORGAM) aerosol model) (Ackermann et al., 1998; Schell et al., 2001) including some aqueous reactions were implemented by Grell et al. (2005) into WRF-Chem. The aerosol size distribution is represented by three size modes (Aitken, accumulation, and coarse modes, assuming a log-normal distribution within each mode) in MADE/SORGAM. In this aerosol model, aerosol species include sulfate, nitrate, ammonium, black carbon (BC), organic matters (OM), sea salt, mineral dust, and water. Different aerosol species within each size mode are assumed to be internally mixed so that all particles within a size mode have the same chemical composition. Aerosol optical properties for scattering (e.g., single-scattering albedo, asymmetry factor, and extinction) are computed as a function of wavelength and three-dimensional position. The Optical Properties of Aerosols and Clouds (OPAC) dataset (Hess et al., 1998) is used for the LW refractive indices of dust, while a constant value of $1.53 + 0.003i$ is used for the SW refractive index of dust following Zhao et al. (2011). Aerosol radiative effect is simulated by the Rapid Radiative Transfer Model (RRTMG) (Mlawer et al., 1997; Iacono et al., 2000) for both short-wave (SW) and long-wave (LW) radiation (Zhao et al., 2011). A detailed description of the computation of aerosol optical properties in WRF-Chem can be found in Fast et al. (2006) and Barnard et al. (2010). The optical properties and direct radiative forcing of individual aerosol species are diagnosed using the method described in Zhao et al. (2013b).

The GOCART dust emission scheme (Ginoux et al., 2001) was coupled with MADE/SORGAM in WRF-Chem by Zhao et al. (2010). As described in Ginoux et al. (2001), the GOCART scheme calculates the dust emission flux G (μg m^{-2} s^{-1}) as

$$G = CSs_p u_{10m}^2 (u_{10m} - u_t)$$

where C is an empirical proportionality constant ($C = 1.0$ in this simulation), S is a source function that defines the potential dust source regions and comprises surface factors, such as vegetation and snow cover, s_p is a fraction of each size class of dust in emission, u_{10m} is
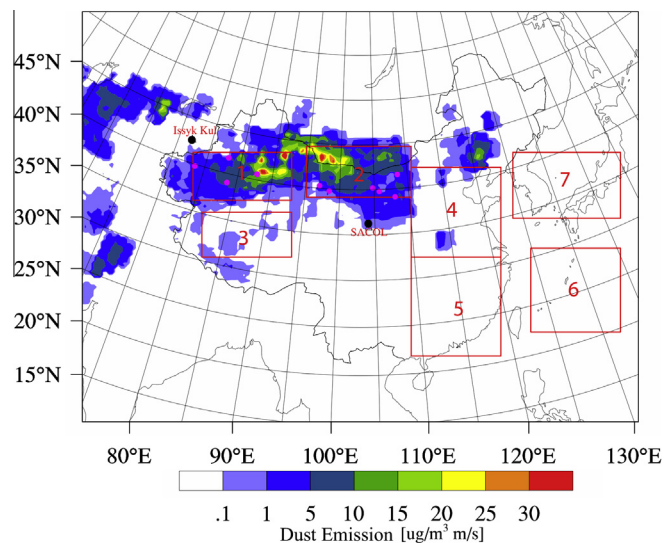

Fig. 1. Modeling domain and spatial distribution of dust emission over East Asia. Seven regions (1. Taklimakan Desert (TD), 2. Gobi Desert (GD), 3. Tibetan Plateau (TP), 4. Northern China, 5. Southern China, 6. East-China-Sea, 7. Korea-Japan) are defined by the red boxes for analysis. Pink dots represent the sites with observed 10 m-winds. Black dots represent the SACOL and Issyk Kul sites.

the horizontal wind speed at 10 m, u_t is the threshold wind velocity below which dust emission does not occur and is a function of particle size, air density, and surface soil moisture. Dust particles are emitted into two log-normal modes (accumulation and coarse) with mass fraction of 15% and 85%, respectively, following Zhao et al. (2010). The volume median diameter and the standard deviation of the two log-normal modes are 2.91 μm and 2.20, respectively, for the accumulation mode, and 6.91 μm and 1.73, respectively, for the coarse mode. The dust mass and number concentrations in each mode are updated during the simulations. The volume mean diameters of each mode are also updated from the predicted mass and number concentrations, while the prescribed standard deviation are kept constant. More details about the coupling of the GO-CART dust emission scheme with WRF-Chem can be found in Zhao et al. (2010). Anthropogenic emissions of carbon monoxide (CO), nitrogen oxides (NOx), SO₂, volatile organic compounds (VOCs), BC, OC, PM₂.₅, and PM₁₀ are from the 2006 emission inventory developed by David Street (http://www.cgrer.uiowa.edu/EMIS-SION_DATA_new/index_16.html). Biomass burning emissions are obtained from the Global Fire Emissions Database, Version 3 (GFEDv3) with monthly temporal resolution and 0.5° spatial resolution (van der Werf et al., 2010).

The simulation domain covers the entire East Asian region (10.7°N–59.8°N, 51.6°E–154.4°E) (Fig. 1) using 138×187 grid points at 36 km horizontal resolution and 35 vertical layers with model top pressure at 100 hPa. The initial meteorological fields and lateral boundary conditions are from the National Center for Environmental Prediction final analysis (NCEP/FNL) data at 1-degree horizontal resolution and 6-h temporal intervals. To reduce the wall clock time for the simulation, the experiment is conducted for each year separately with a start date of December 15 from the prior year to allow model spin up, and the simulations for each year are concatenated to cover the 5-year period of 2007–2011 (referred to as the simulation period hereafter). The modeled u- and v-component winds and atmospheric temperature are nudged above the PBL towards the NCEP/FNL analysis data with a nudging time scale of 6 h over the entire domain to produce a more realistic simulation of the large-scale circulation (Stauffer and Seaman, 1990). No nudging is applied within the PBL in order to avoid inferences with resolved mesoscale forcing and topography forcing near the surface in simulations. The Noah land surface model (Chen et al., 1996; Chen and Dudhia, 2001) and the Yonsei University (YSU) planetary boundary scheme (Hong et al., 2006) are used in this simulation. The Morrison two-moment microphysics scheme (Morrison et al., 2005) and Kain–Fritsch convective scheme (Kain and Michael Fritsch, 1990; Kain, 2004) are used to represent cloud microphysics and convection processes. The convective transport of gases and aerosols was coupled with the Kain–Fritsch convective scheme by Zhao et al. (2013a). The chemical initial and boundary conditions are from the default profiles in WRF-Chem, which are the same as those used by McKeen et al. (2002) and are based on averages of mid-latitude aircraft profiles from several field studies over the eastern Pacific Ocean.
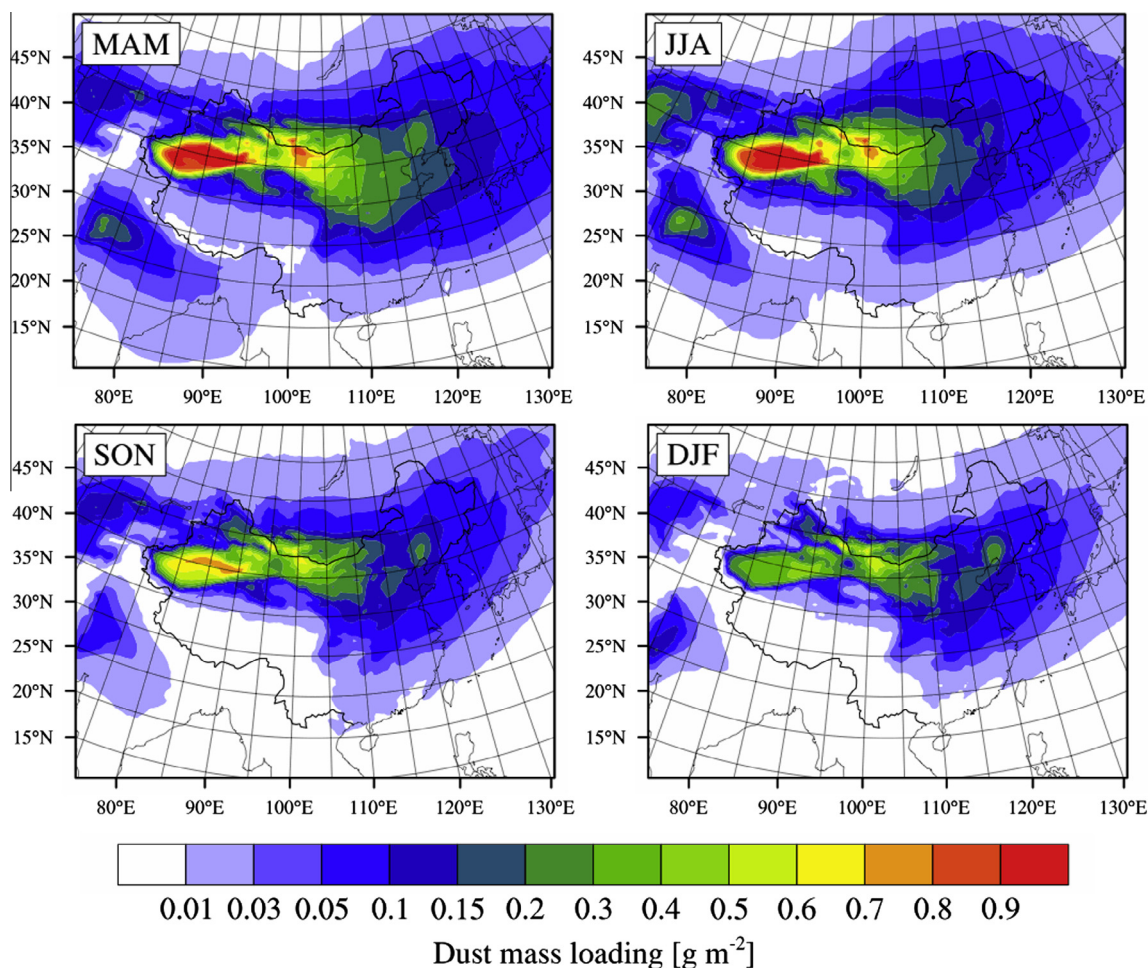
Fig. 2. The spatial distribution of seasonally averaged dust column concentration over East Asia for spring (March–April–May, MAM), summer (June-July–August, JJA), autumn (September–October-November, SON) and winter (December-January–February, DJF) in 2007–2011 from the WRF-Chem simulations.
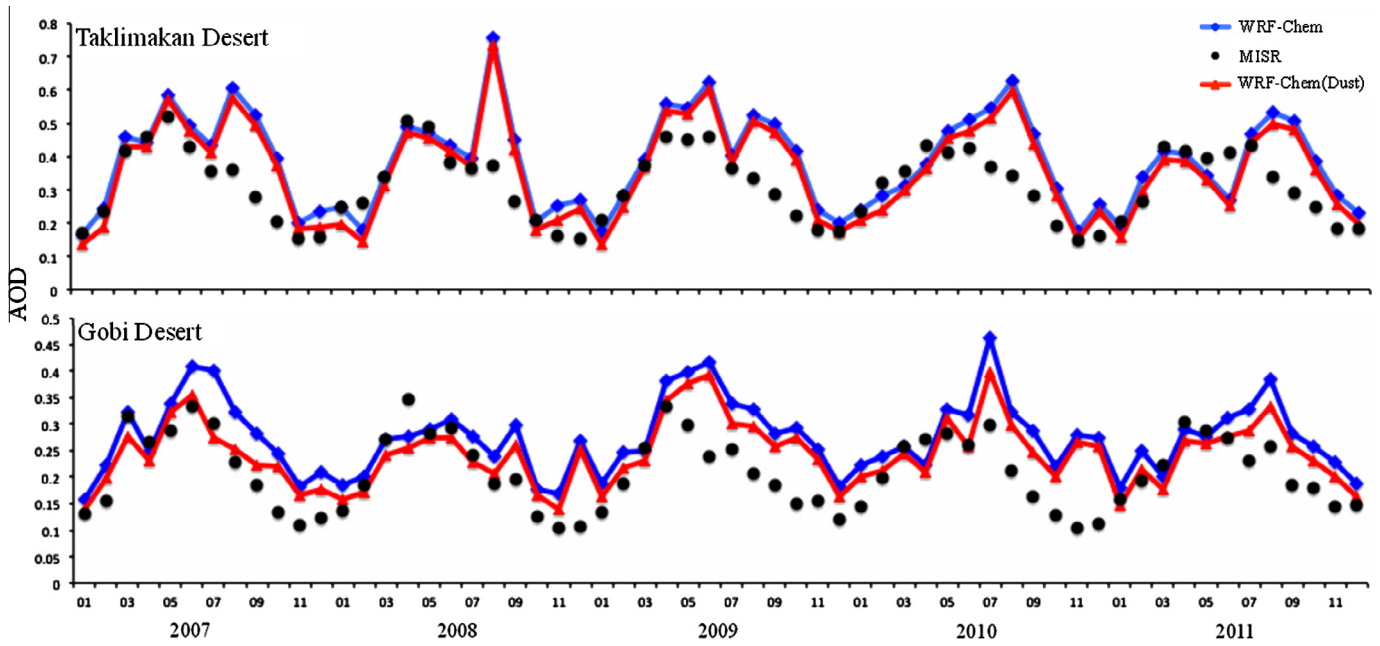
Fig. 3. Monthly total AOD over the TD and GD from the MISR retrievals (black dots) and the WRF-Chem simulations (solid lines) for 2007–2011. Both total AOD (blue line) and dust AOD (red line) from the simulations are shown.

3. Observations

3.1. Semi-Arid Climate Observatory and Laboratory (SACOL)

SACOL, established in late 2005, is located at the southern bank of the Yellow River in the Gansu province in Northwest China

(35.57°N, 104.08°E, elevation: 1970 m). The area is covered mainly by quaternary aeolian loess, where more than 70% of the aerosols are transported from the TD and the Gobi Deserts (GD) by the prevailing westerly winds. SACOL provides a long-term continuous of aerosol optical depth (AOD), aerosol vertical profile, single scatting albedo (SSA), and aerosol size distribution. Detailed descriptions of
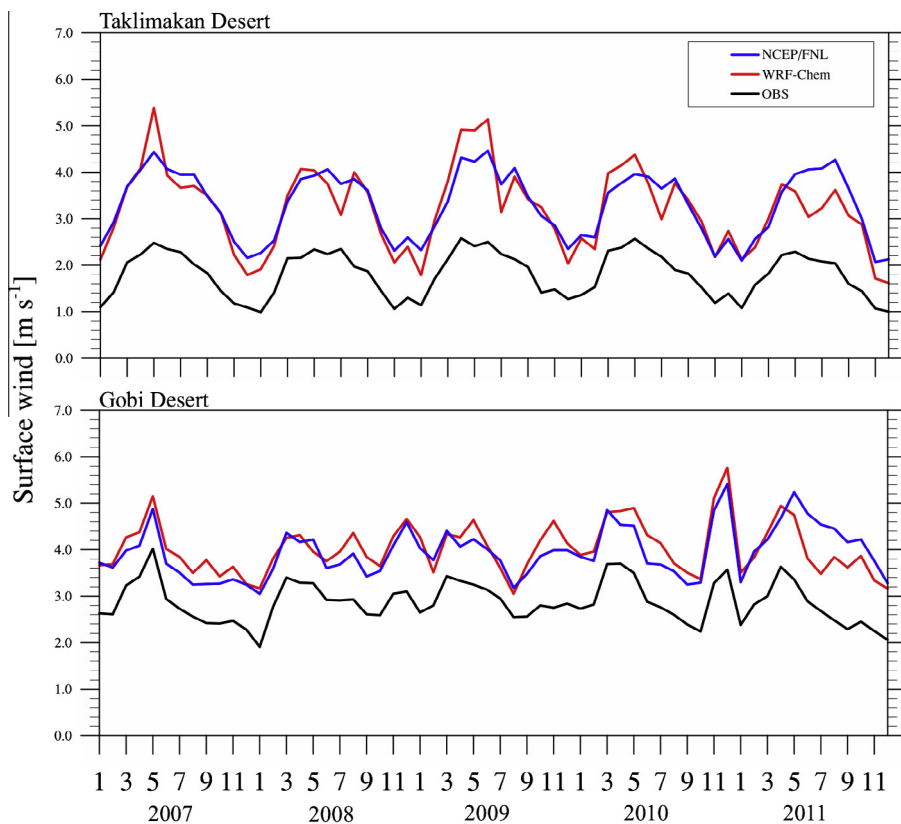
Fig. 4. Monthly mean 10-meter winds averaged at the observation sites over the TD and GD (Fig. 1) from observations (black lines) and NCEP/FNL reanalysis data (blue lines) and WRF-Chem simulations (red lines) for 2007–2011.
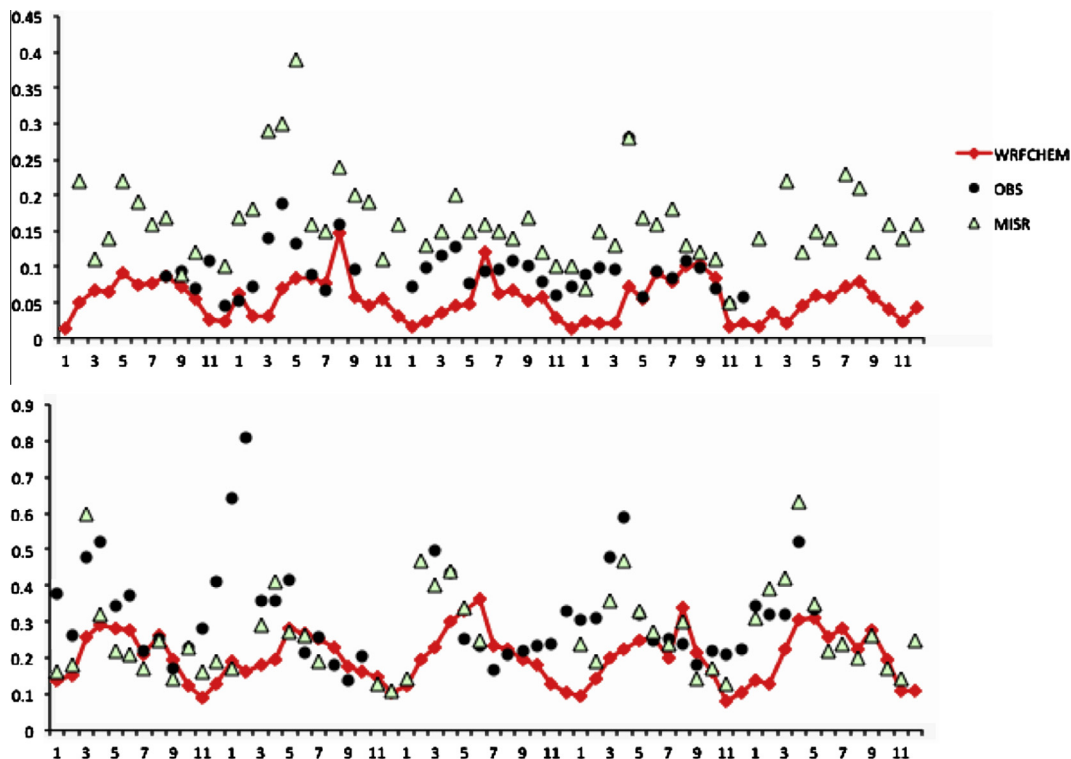
Fig. 5. Monthly variations of AOD at 550 nm from the AERONET (black dots) and MISR retrievals (green triangles) and the corresponding WRF-Chem simulations (red lines) at the Issyk Kul (top panel) and SACOL (second panel) sites (Fig. 1) for 2007–2011.

this site and the related instruments are given by Huang et al. (2008b) and Bi et al. (2011). This study mainly uses the measurements of AOD, aerosol extinction profiles, and aerosol size distributions.

3.1.1. Aerosol optical depth

SACOL is one of the Aerosol Robotic Network (AERONET) sites over Loess Plateau in Northwestern China. The automatic sun and sky scanning radiometer (CIMEL Sunphotometer) makes measurements of the direct sun and diffuse sky radiances within

the spectral range of 340–1020 nm (Holben et al., 1998). The automatic tracking sun and sky scanning radiometer makes direct sun measurements with a 1.2 full field of view every 15 min in eight spectral channels at 340, 380, 440, 550, 675, 870, 940 and 1020 nm. In addition, AOD retrieved at another AERONET site at Issyk Kul (42°N, 76°E) (Holben et al., 1998) is also used in this study.

3.1.2. Aerosol extinction vertical profile

Vertical distribution of aerosol extinction coefficient is measured using a Micro-Pulse Lidar system operating at a wavelength
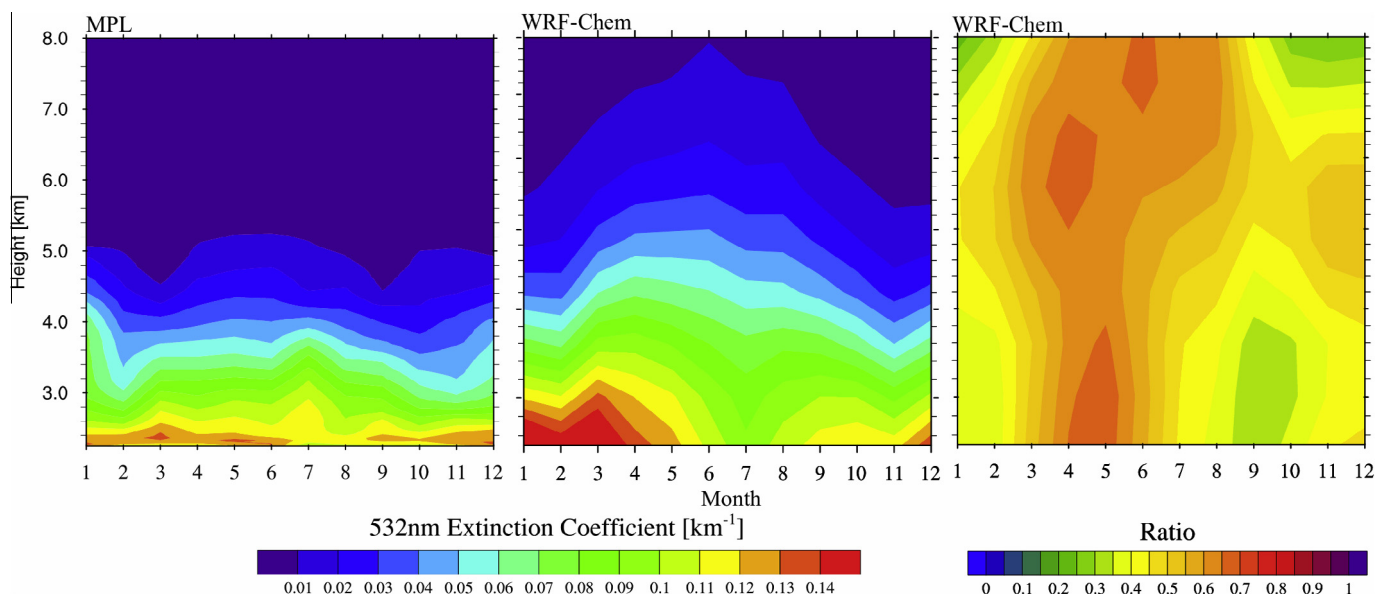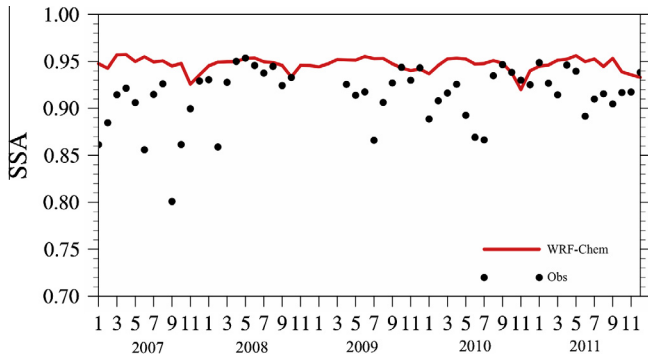

Fig. 6. Monthly vertical profiles of aerosol extinction coefficients at 532 nm for 2007–2011 from the MPL retrievals (right panel) and the corresponding WRF-Chem simulation (middle panel), and the dust contribution (dust extinction coefficient /total aerosols extinction coefficient) from the WRF-Chem simulation (right panel).

Fig. 7. Monthly variations of SSA at 532 nm at the SACOL site from the AEROENT retrievals (black dots) and the WRF-Chem simulations (red line) for 2007–2011.

Fig. 8. Seasonal variations of aerosol size distributions in the total atmospheric column at the SACOL site from the observations (dots) and the corresponding WRF-Chem simulations (solid lines).

of 527 nm (MPL-4, Sigma Space) (Spinhirne, 1993). MPL lidar is a safe, compact, and maintenance-free lidar system originally developed by for acquiring long-term data sets of backscatter profiles of aerosols and clouds (Welton et al., 2001). Continuous aerosol and cloud measurements are acquired with a 75 m range resolution at a 1 min time average (Huang et al., 2008b).

3.1.3. Aerosol single scattering albedo (SSA)

Aerosol single scattering albedo is retrieved from AERONET data following the approach discussed in detail by Dubovik and King (2000) and Dubovik et al. (2002). The error in the retrieved aerosol parameters is described by Dubovik et al. (2002) for urban-industrial, biomass burning and desert dust aerosols.

3.1.4. Aerosol size distributions

The particle sizer (APS-3321) acquires the aerosol effective particle diameter in the surface layer using a dual-parallel laser and low-frequency particle accelerator by measuring the time a particle takes to cross the laser beam. It measures the light-scattering intensity by examining each particle's side-scatter signal intensity and provides an accurate count size distribution for aerosols with effective diameters of 0.53–20 µm, and light-scattering intensity for particles ranging from 0.3 to 20 µm (Zhou et al., 2012).

3.2. MISR

The AOD data from the Multi-angle Imaging SpectroRadiometer (MISR) aerosol Level 3 retrievals are also used. MISR on board the NASA Terra platform has been producing AOD globally since February 2000 and passing over the equator at 10:45 LT during daytime. The resolution of the Level 3 MISR AOD products is 0.5° × 0.5°. It can retrieve aerosol properties even over highly reflective surfaces like deserts (Martonchik et al., 2004). A detailed description of MISR aerosol retrieval is given by Martonchik et al. (1998, 2002). For comparison, the model results are sampled in the same overpass time as MISR on Terra.

4. Results and discussion

4.1. Evaluation of dust simulation

The simulated dust-emission fluxes over East Asia averaged for 2007–2011 reveals dust sources mainly over the two major deserts of West China (i.e., TD and GD) and some arid areas of North China (Fig. 1). The maximum dust emission fluxes reach $30\ \mu g\ m^{-2}\ s^{-1}$ over the TD and GD. There are also small amounts of dust emissions (0.1–$1\ \mu g\ m^{-2}\ s^{-1}$) over the TP. Seven sub-regions are defined
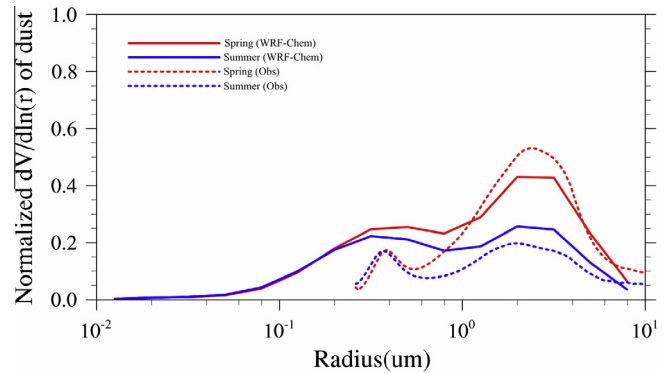
in the red boxes for further analysis of dust mass balance in Section 4.2. These seven sub-regions are selected to represent the dust source regions and outflow regions. In this study, only the TD and GD are selected as the dust source regions over East Asia, because other dust sources are relatively small compared to these two (Sun et al., 2001). The annual average dust column concentration over East Asia in 2007–2011 from the simulations shows the high concentration over the dust source regions with large dust-emission fluxes (Fig. 2). Although dust emissions over the TD and GD are similar, the model simulates higher dust column concentration over the TD. The TD and GD dusts are transported downwind (i.e., eastward) to East China, Japan, Korea, and Pacific Ocean. All seasons have similar spatial distribution of dust column mass concentration over East Asia, but the amount is higher in spring and summer than fall and winter. The dust column mass concentration in spring and summer over the TD and GD are comparable. However, the eastward dust transport is stronger in spring than summer because of the stronger prevailing winds.

To evaluate the model performance in simulating dust column mass concentration over East Asia, we first compare the simulated dust column concentration over the dust source regions against measurements. The WRF-Chem simulations well capture the MISR retrieved inter-annual and seasonal AOD variations over the TD and GD (region 1 and region 2 in Fig. 1) in 2007–2011. Satellite retrievals are used instead because in situ measurements over the TD and GD are scarce. From the MISR retrievals and the WRF-Chem simulations, the monthly AOD at 550 nm averaged over the TD and GD show small inter-annual but clear seasonal variations (Fig. 3). Over the TD, the MISR retrievals show the highest AOD of 0.43 in spring and the lowest AOD of 0.22 in winter. The retrievals over the GD show similar seasonal variation with the highest AOD of 0.29 in spring and the lowest AOD of 0.15 in winter. From the simulated total aerosol AOD and dust AOD, dust is the dominant aerosol species over the TD (~98%) and GD (~95%). The model simulates consistent results with high AOD of 0.44 and 0.29 in spring and low AOD of 0.24 and 0.21 in winter over the TD and GD, respectively.

It is noteworthy that the model overestimates the AOD in summer and fall, especially over the TD (summer: 0.13; fall: 0.08). One possible reason for the overestimations of simulated dust AOD in summer and fall could be the biases in simulating surface wind speed. The 10-m winds averaged at the observation sites over the TD and GD from observations, reanalysis data, and WRF-Chem simulations are shown in Fig. 4. Although simulations overestimate the magnitude of observed 10-m wind speed over the TD and GD, but they reproduce the observed seasonal and inter-annual variations quite well (Fig. 4). Daily wind speed observations in the 10

in situ sites (shown in Fig. 1) during 2007–2011 were obtained from the Chinese National metrological Center (CNMC). An overestimation in simulated surface winds in WRF 3.3.1 is a common issue due to model limitations in representing turbulence processes and subgrid variations in terrain and land surface type (Hanna et al., 2000), which may be improved in the newer version of WRF (e.g., v3.5) through using the surface drag parameterization (Jiménez and Dudhia, 2012; Mass and Ovens, 2011). However, the seasonal and inter-annual variations of simulated AOD over the TD and GD is consistent with the comparison of 10-m winds (Figs. 3 and 4), so the overestimation of the simulated AOD in summer and fall may not be related to the biases in seasonal variations of simulated surface winds. Since the simulated large-scale winds in the free troposphere are consistent with the reanalysis data (not shown), the overestimated AOD may also not be related to errors in dust-transport modeling. The difference between observed and simulated winds might be related to failure of the

dust-emission parameterization is not able to capture the seasonal variation of dust-emission fluxes. This issue is not investigated in this study and should be examined further.

In addition to the evaluation of the simulated AOD over the TD and GD, the AERONET and MISR observations are compared with the simulated AOD at two AERONET sites (Issyk Kul and SACOL in Fig. 1) near the dust-source regions. Generally speaking, AERONET retrieval has smaller uncertainties than that of MISR (Petrenko and Ichoku, 2013). At the Issyk Kul site, the monthly variations of AOD at 550 nm from the AERONET and MISR retrievals were similar lumped by seasons, with relatively high AOD in spring and summer and low AOD in fall and winter (Fig. 5). However, the MISR retrieved AOD has an annual average of ~0.16 that is higher than the annual average of ~0.1 from AERONET. The model well captures the seasonal variations of the observed AOD, but underestimates AOD, especially in winter, which may be due to local emissions from residential burning in winter that is not well
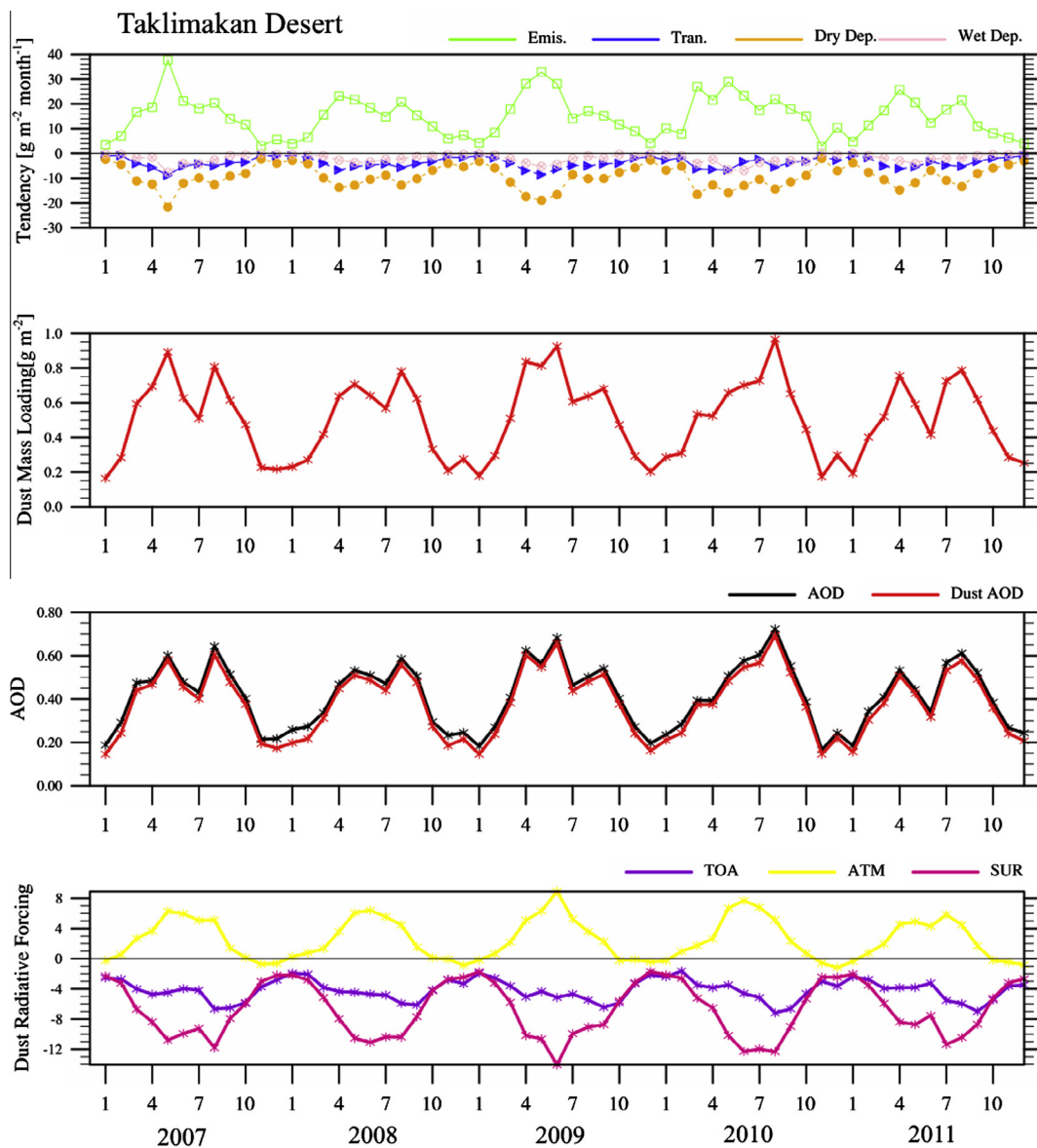
Fig. 9a. Monthly averaged contributions of emission (Emis.), transport (Tran.), dry (Dry Dep.) and wet deposition (Wet Dep.) to dust mass balance (top panel), dust column concentration (2nd panel), total aerosol and dust AOD (3rd panel), and dust raidiative forcing (Dust RF) (bottom) at the top of atmosphere (TOA), in the atmosphere (ATM), and at the surface (SUR) for 2007–2011 over the Taklimakan desert. For dust budget analysis, positive value denotes positive contributions to dust mass balance. Units: g m^{-2} month^{-1}. For dust direct radiative forcing, positive values at the TOA and SUR represent downward radiative fluxes, and represent radiative warming in the ATM. Unit: W m^{-2}.

treated in the model. At the SACOL site, the MISR retrieved AOD is more consistent with that from the AERONET in both seasonal variation and annual mean (Fig. 5). The MISR retrieved annual AOD of 0.26 is comparable to the AERONET measurement of 0.30, and both show relatively high AOD in spring and summer and relatively low AOD in fall and winter. The model generally reproduces the seasonal variations of the observed AOD. Again, the model underestimates AOD particularly in winter, which is likely due to large amounts of pollutants from residential burning transported from Lanzhou city in winter (Wang et al., 2010).

Besides column-integrated dust AOD, vertical extinction profile of dust is also critical in the assessment of dust radiative forcing (Claquin et al., 1998). The micro-pulse lidar (MPL) observations of aerosol extinction coefficients at 532 nm at the SACOL site (2007–2011) provides an opportunity to evaluate the vertical structure of monthly dust distributions near the source regions with respect to the corresponding WRF-Chem simulations (Fig. 6). A relatively high aerosol extinction coefficient (up to 0.15 km^{-1}) was distributed in the lower atmosphere (below 4.0 km). There is clear seasonal variation of the aerosol extinction

coefficient near the surface with a minimum in summer. The simulation generally captures the retrieved seasonal variations of vertical aerosol extinction profiles with an annual minimum surface extinction coefficient in summer because surface relative humidity is the lowest in summer at the SACOL site (not shown). The model simulation indicates a high dust contribution (up to 70%) to the aerosol extinction profiles up to 8 km in spring. In other seasons, dust contribution is relatively small (<40%) near the surface (Fig. 6). The magnitude of simulated aerosol extinction coefficient is higher than that of observation from the MPL retrievals near the surface in winter. However, at the SACOL site in winter, WRF-Chem simulated AOD is lower than the AERONET retrievals (Fig. 5). MPL retrievals underestimate AOD compared with AERONET retrievals in winter. This underestimation is likely due to the uncertainty in the liar ratio during retrieving. The MPL retrievals of aerosol extinction profiles are complicated by the fact that the lidar equation contains two unknown factors that are backscattering and extinction coefficients. In order to obtain an analytical solution to the lidar equation, it has been a common practice to assume that these parameters are related by the lidar ratio (Fernald,
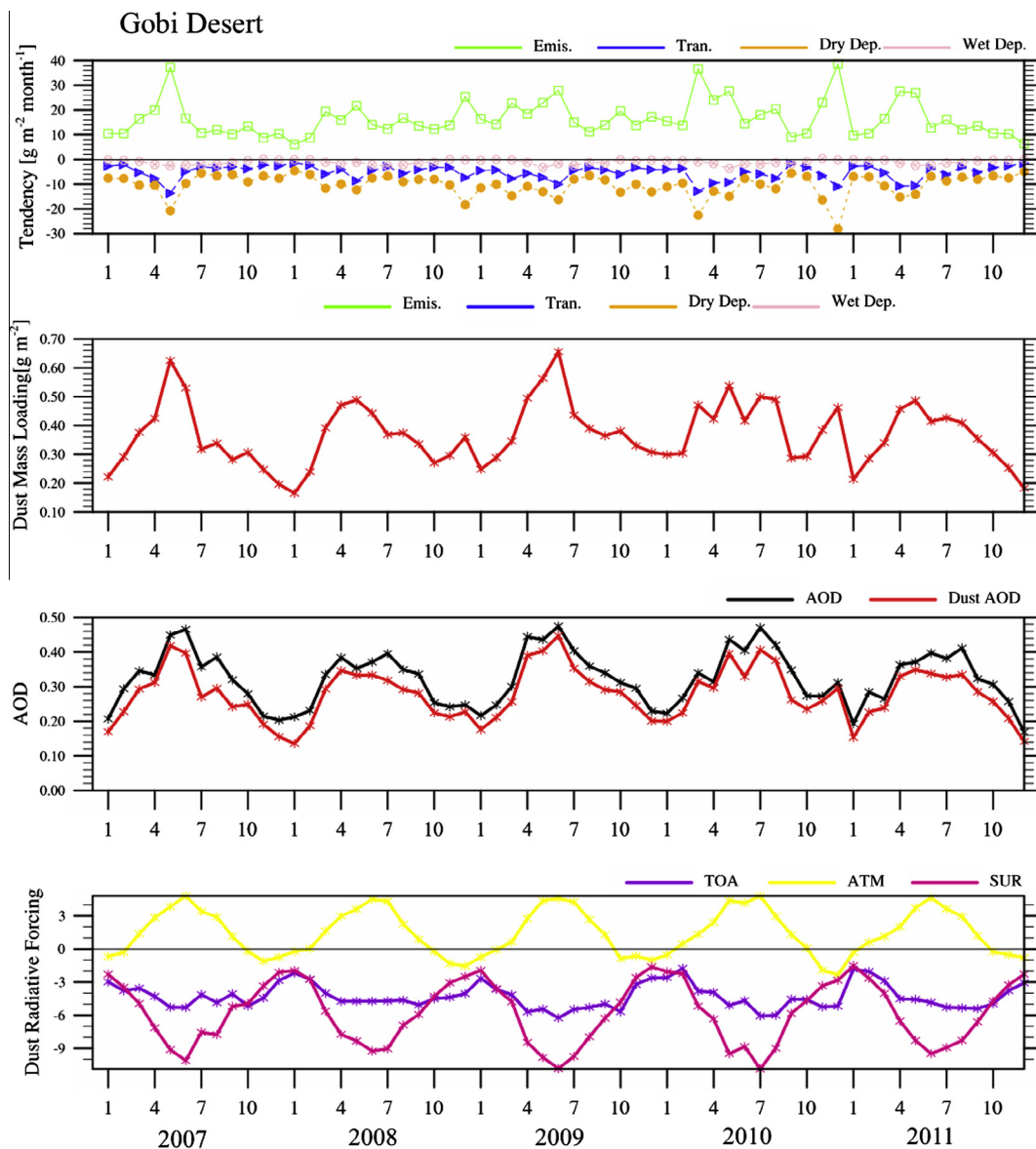

Fig. 9b. Same as Fig. 9a over the Gobi desert.

1984). Lidar ratio is a very important optical parameter in the aerosol characterization, which depends on intensive aerosol properties such as chemical composition, size distribution, and particle shape (ZW Huang et al., 2010; Zhou et al., 2013). We use a single lidar ratio as 50 sr in the MPL retrievals, which mainly present the dust optical properties. In winter, dust contribution is relatively small (<40%) near the surface (Fig. 6). Therefore, BC or other kinds of aerosols may increase the biases in the MPL retrievals at SACOL in winter.

Dust is one of few absorbing aerosol species in the atmosphere. Dust absorptivity is an important factor affecting the heating rate of the atmosphere. The aerosol single scattering albedo (SSA) can be used to characterize aerosol absorption properties. The comparison of the monthly SSA at 532 nm at the SACOL site from the AERONET retrievals and the WRF-Chem simulations for 2007–2011 is shown in Fig. 7. The simulation, with a SSA value of 0.94, generally captures the retrieved background (annual average of 0.91), but it fails to reproduce the observed large temporal variation. Model generally captures SSA variations around 0.95, but fails to reproduce the low SSA values around 0.90 or even lower. As shown, observed SSA at 532 nm reached as low as 0.85, which is

unlikely driven by dust even if the refractive index of dust was tuned. It is more likely that the observed low SSA is affected by variations of local anthropogenic emissions that is difficult to be captured by the simulations with 36 km resolution and a half-degree resolution of anthropogenic emissions. A small bias in simulating BC concentrations can result in a significant change in SSA (Barnard et al., 2010). To better evaluate the dust optical properties, the simultaneous observations of BC concentrations with SSA would help. Furthermore, the AERONET retrieved SSA may also have low biases (Osborne et al., 2008).

The size distribution of dust particles in the atmosphere is also strongly influences dust direct radiative forcing but in ways difficult to quantify (Zhao et al., 2010, 2013a). We compared the normalized volume-size distributions of aerosol particles at the SACOL site from the observations and WRF-Chem simulations in spring and summer of 2007–2011 (Fig. 8). The aerosol size distributions are only compared in spring and summer because dust has larger contributions to total aerosols in these two seasons at the SACOL site (Fig. 6). The observed aerosol size distributions show apparent bimodal pattern with one peak in the fine mode at 0.4 μm and the other in the coarse mode at 3 μm in radius. In
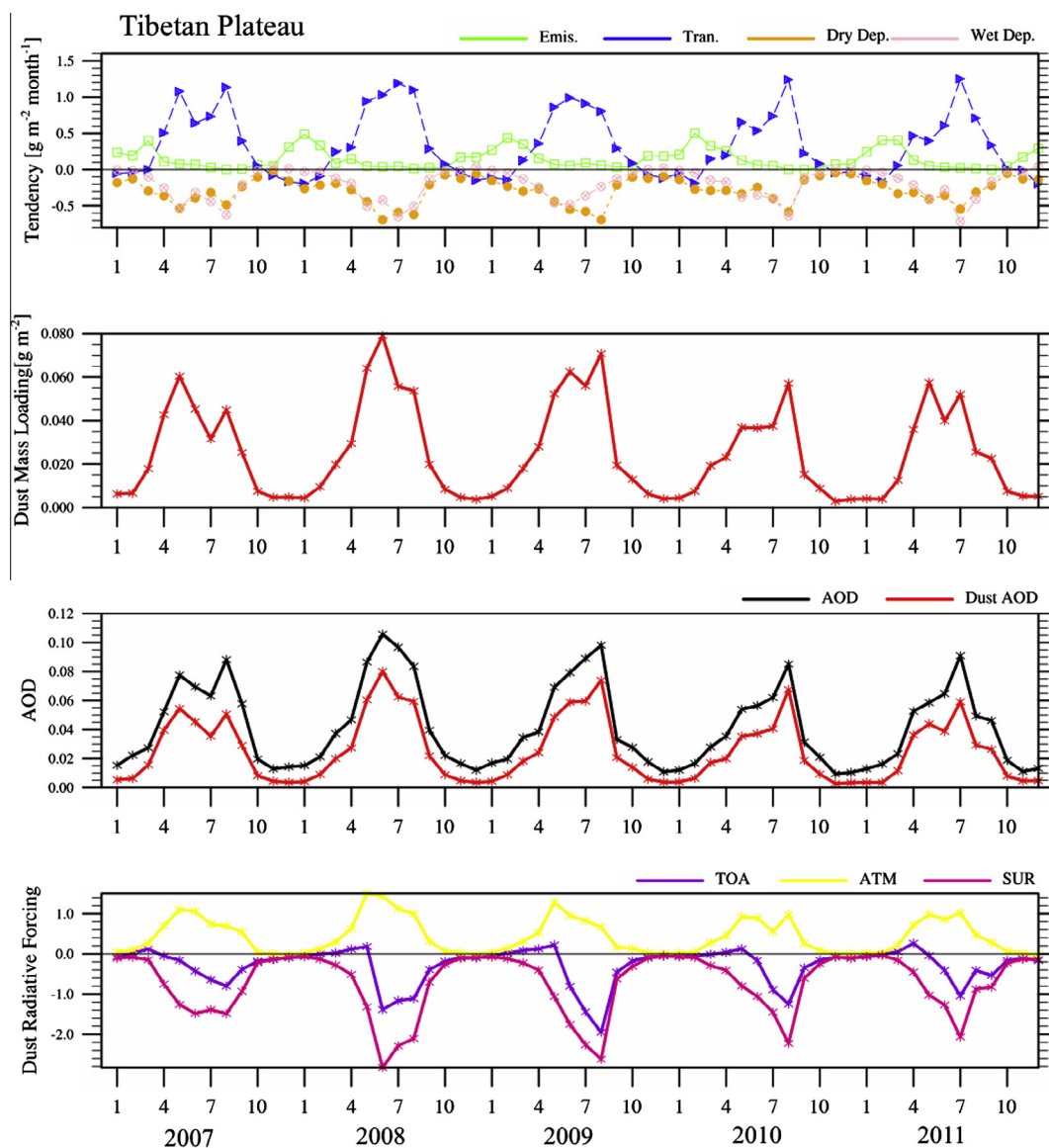

Fig. 9c. Same as Fig. 9a over the Tibetan Plateau.

general, the coarse-mode peak is higher than the fine-mode peak. It shows relatively more coarse-mode particles and fewer fine-mode particles in spring than in summer, indicating that dust is a more dominant aerosol species in spring than in summer at the SACOL site. The model also captures the bimodal pattern of the aerosol size distributions and its seasonal variations. However, the simulation tends to overestimate the fine-mode aerosol particles and underestimates the coarse-mode aerosol particles in both seasons compared to the retrievals. This difference is likely due to uncertainties in modal size parameterization that is used in this study. Zhao et al. (2010, 2013a) also found that WRF-Chem with the modal size parameterization with the prescribed standard deviation underestimates coarse-mode aerosol particles and overestimates fine-mode aerosol particles compared to observations and simulations using the same dry deposition parameterization but with 8-bin size representation.

4.2. Dust mass balance and direct radiative forcing

To understand better the dust mass balance and its determining factors in the corresponding regimes, seven sub-regions are defined in this study. The monthly contributions of emission, transport, dry and wet deposition, dust column concentration, total aerosol and dust AOD, and dust direct radiative forcing for 2007–2011 were averaged over seven sub-regions of East Asia (Figs. 9a–9g). As shown in Fig. 1, regions 1 and 2 represent the typical dust source regions (TD and GD). It is noteworthy that TD and GD are two dominant source regions of dust raised from China and its surrounding regions (Sun et al., 2001), which is primarily transported toward the southeast and then the northeast (Shao et al., 2013). Therefore, we just focused on these dust source regions in the study. In addition, region 3 represents the Tibetan Plateau (TP) that plays an important role in the climate system over East Asia; regions 4 and 5 represent North and South China, where dust storm may have significant impact on regional climate and human health; region 6 represents the East Asian dust outflow region with dust deposition into ocean; region 7 represents the East Asian dust outflow region affecting Korea and Japan.

Over the TD and GD, dust emission is the only factor contributing positively to the dust mass balance, while transport as well as dry and wet depositions are sinks of dust in the atmosphere (Figs. 9a and 9b). The dust emission has smaller seasonal variations than dust column concentration over both regions. Dust column concentration, emission, and sink are found to be higher over the
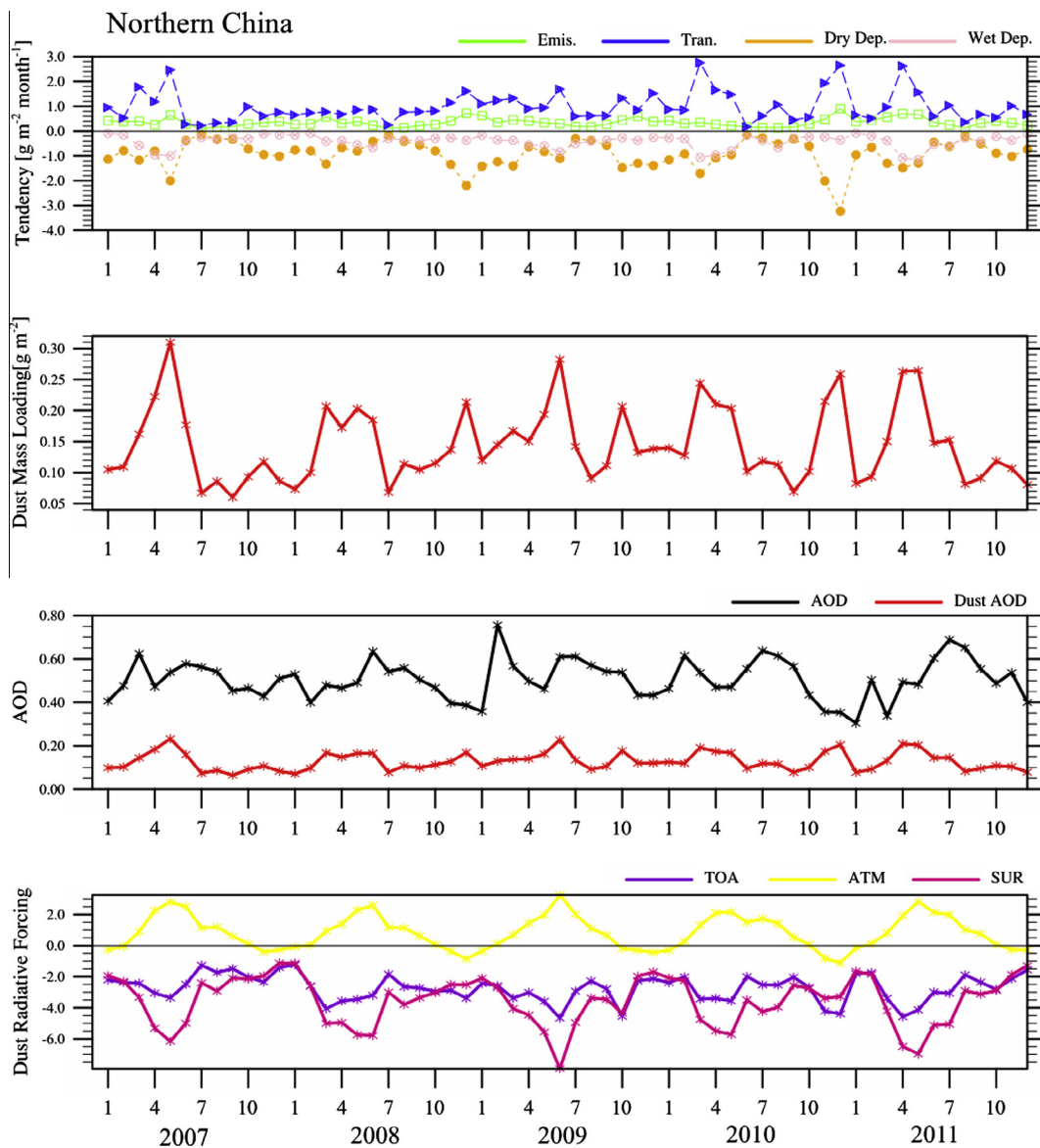

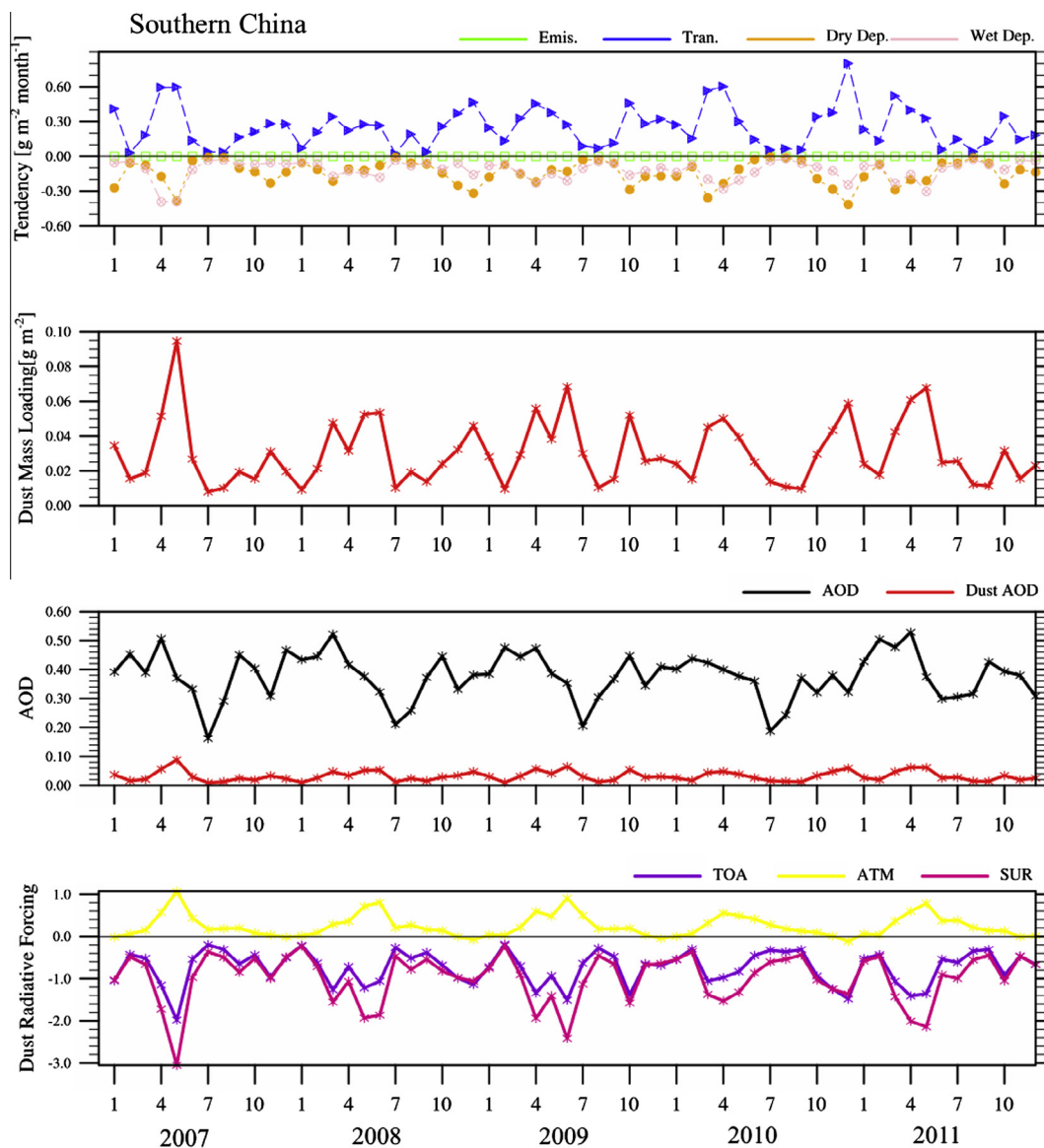**Fig. 9d.** Same as Fig. 9a over North China.

Fig. 9e. Same as Fig. 9a over South China.

TD than over the GD. The column concentration of TD dust has larger seasonal variations but smaller inter-annual variations than the GD dust, which is mainly determined by seasonal and inter-annual variations of dust emissions. Over both regions, dry deposition is the largest sink of dust, following by transport and wet deposition. It is interesting to note that wet deposition is comparable to transport over the TD, but wet deposition over the GD is much smaller. Larger dust emission over the TD results in larger dust column concentration and AOD than over the GD. In addition, the dust contribution to the total aerosol AOD is larger over the TD than the GD. Both TD and GD dust direct radiative forcing have relatively small inter-annual variations but large seasonal variations with maximum values in late spring and early summer. Dust results in a surface cooling of up to −14 and −10 W m^{-2}, atmospheric warming of up to 9 and 2 W m^{-2}, and TOA cooling of −5 and −8 W m^{-2} over the TD and GD, respectively.

Over the TP, dry and wet depositions are the primary and comparable sinks of dust in the atmosphere with obvious seasonal variations (Fig. 9c). Both dry and wet depositions of dust reach a maximum in summer. Both emission and transport can contribute positively to the dust-mass balance over the TP. Emission is the

major dust source over the TP in winter and early spring. On the contrary, transport is the major dust source in seasons other than winter with a maximum in summer. In fact, transport has a negative contribution to the dust-mass balance in winter. The dust column concentration has an evident seasonal variation with a peak in late spring and summer mainly controlled by the seasonality of dust transport. The mechanism of summer transport of TD dust to the TP has been identified and examined by Chen et al. (2013). It can be seen that dust has a dominant contribution to AOD over the TP except in winter, and the maximum AOD over the TP occurs in summer, which is consistent with the case study analyzed by Huang et al. (2007). The seasonal variation of dust direct radiative forcing also shows a peak in summer. Dust results in a surface cooling of up to −3 W m^{-2}, atmospheric warming of up to 1.4 W m^{-2}, and TOA cooling of −2 W m^{-2} over the TP. The inter-annual difference of dust column concentration and its direct radiative forcing can reach 25% of the long-term mean during 2007–2011.

North and South China are two regions often affected by the dust transported from the west. Transport is the dominant source of dust over both regions, even though there are small amounts of dust emission over North China (Figs. 9d and 9e). The dust column
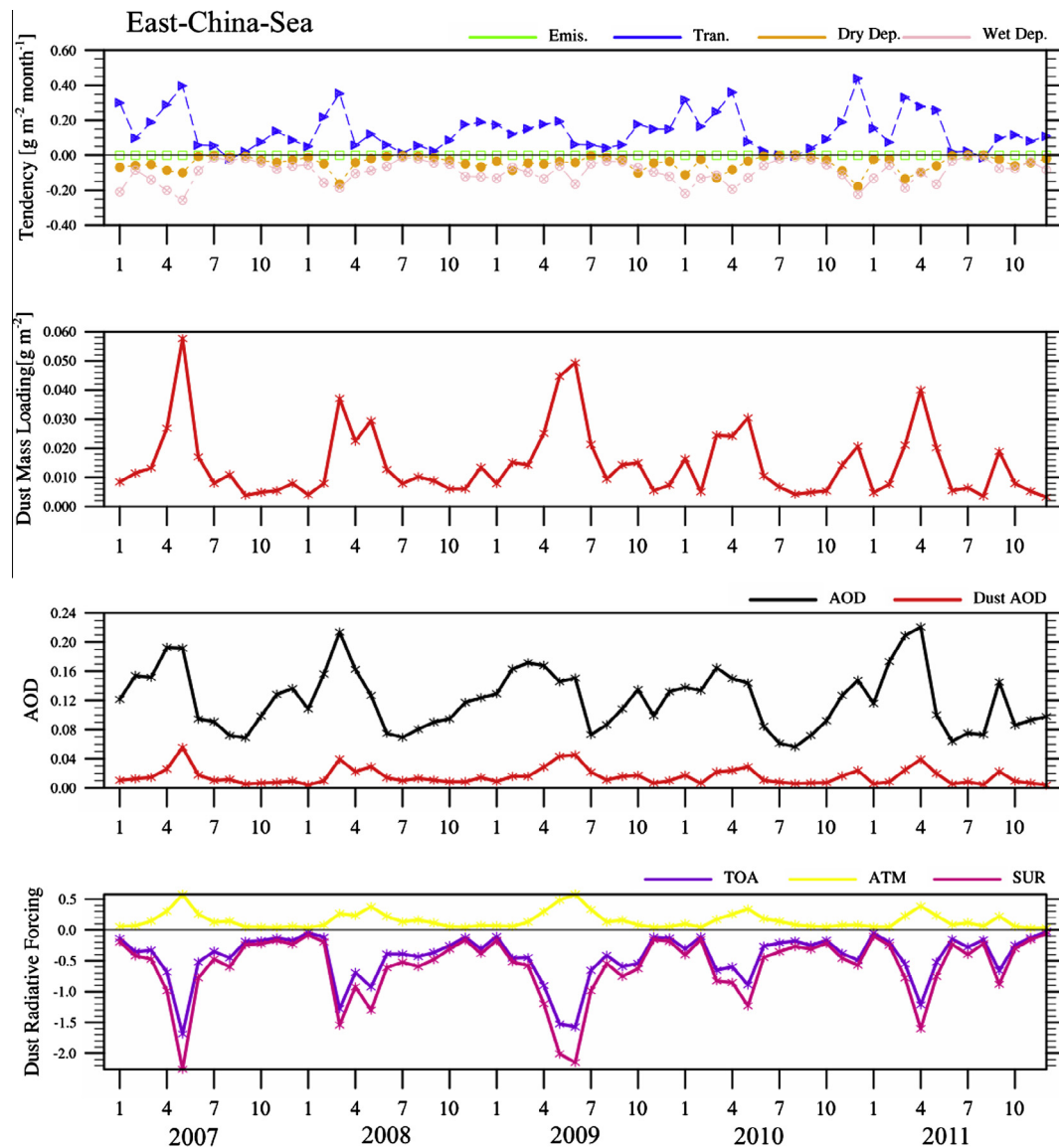
Fig. 9f. Same as Fig. 9a over East China Sea.

concentration is higher over North China than South China due to larger dust transport. The seasonality of dust column concentration over the two regions is not as evident as over the TD, GD, and TP. Although dust column concentration is generally high in spring, there are also some peaks in winter in both regions resulting from the high dust transport. Dry and wet depositions are two sinks of dust in the atmosphere in both regions. Dry deposition is larger than wet deposition over North China, but dry deposition is comparable to wet deposition in South China due to the relatively humid climate. The dust contribution to the total AOD is relatively small (<30%) due to the high loading of anthropogenic aerosols over both regions, especially in South China. Again, dust AOD over the two regions has small seasonal variations. However, the dust direct radiative forcing has a more evident seasonal variation with the maximum in late spring. Dust results in a surface cooling of up to -7 and $-3\,W\,m^{-2}$, atmospheric warming of up to 4 and $1\,W\,m^{-2}$, and TOA cooling of -3 and $-2\,W\,m^{-2}$ over North and South China, respectively.

We focused on East Asian dust transport and deposition in two outflow regions because deposition over the East China Sea may affect the ocean and dust transport over Korea and Japan could affect air quality. Dust transport brings East Asian dust over the ocean

and Korea–Japan, and dust is removed by dry and wet depositions (Figs. 9f and 9g). The dry and wet depositions are comparable over both outflow regions. Over these two regions, both dust column concentration and dry and wet deposition have evident seasonal variations with a maximum in spring, and the inter-annual variation as much as 50%. The dust column concentration is higher over Korea-Japan than East China Sea. In addition, the dust contribution to the total AOD is smaller over the East China Sea (<15%) than over Korea-Japan (~40%) due to the outflow of high concentration of anthropogenic aerosols from China over the East China Sea (Bennartz et al., 2011). Dust results in a surface cooling of up to -2 and $-5\,W\,m^{-2}$, atmospheric warming of up to 0.5 and $2\,W\,m^{-2}$, and TOA cooling of -1.5 and $-3\,W\,m^{-2}$ over the East China Sea and Korea–Japan, respectively. The dust direct radiative forcing in both outflow regions has a maximum in spring.

5. Discussion and conclusions

In this study, the dust mass balance and its direct radiative forcing over East Asia are investigated together with an estimate of the dust lifecycle contributions from various physical processes
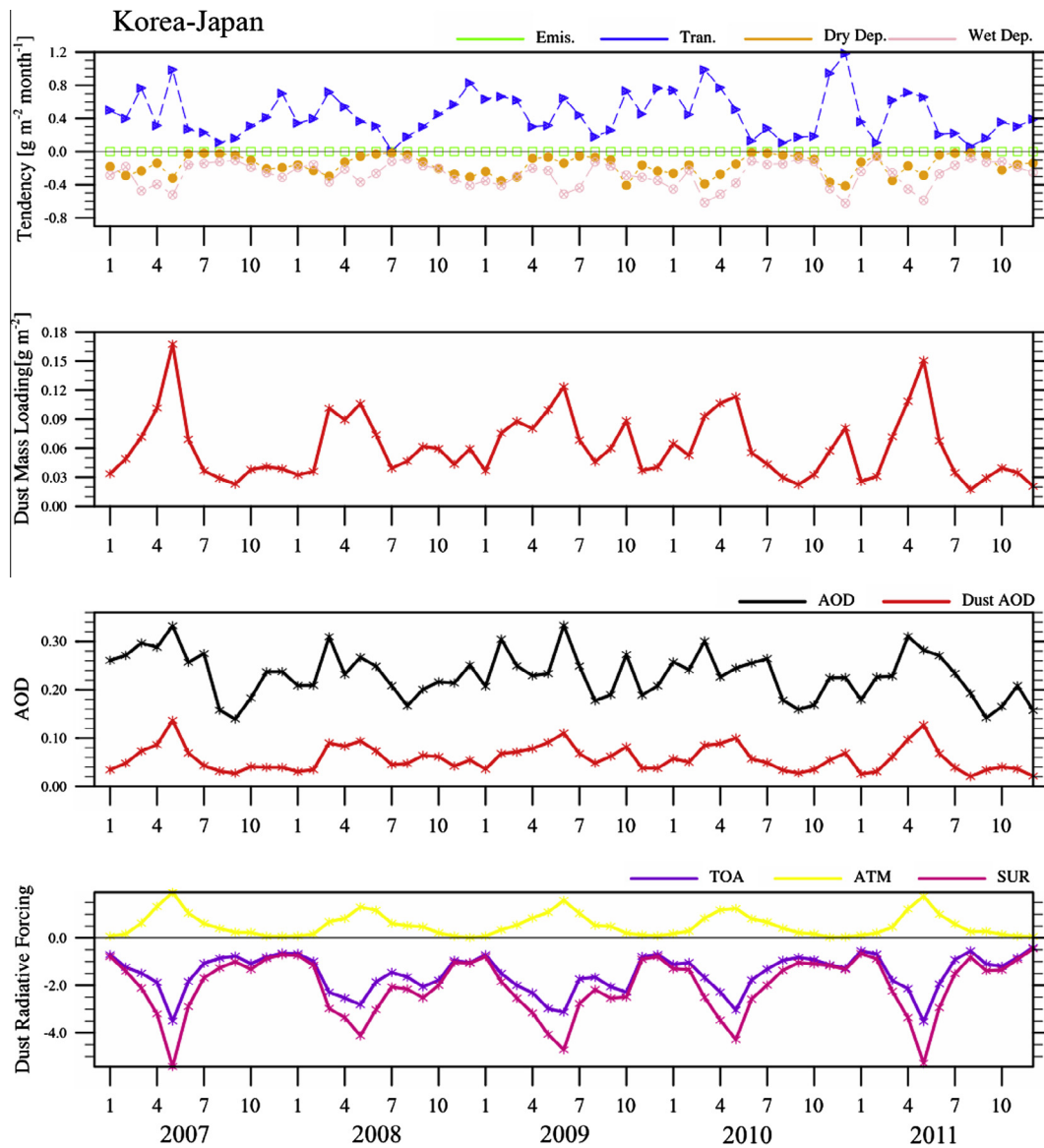
Fig. 9g. Same as Fig. 9a over Korea-Japan.

Table 1
WRF-Chem simulated all-sky direct radiative forcing of dust aerosols in seven regions over the East Asia in 2007–2011.[a]

	[b]Region 1	Region 2	Region 3	Region 4	Region 5	Region 6	Region 7
TOA	−4.2	−4.3	−0.3	−2.7	−0.7	−0.4	−1.5
ATM	2.5	1.4	0.4	0.8	0.2	0.2	0.5
BOT	−6.7	−5.7	−0.7	−3.5	−0.9	−0.6	−2.0

[a] "TOA" represents "top of atmosphere". Positive means downward direction for TOA and surface, and absorption/heating for atmosphere.
[b] Region 1–7 are shown in Fig. 1.

(e.g. dust emission, transport, and dry and wet deposition) using the WRF-Chem model at a horizontal resolution of 36×36 km^2 and online calculation of dust emissions. The simulation runs from 20 December 2006 to 31 December 2011 covering East Asia. Both Dust SW and LW direct radiative effect are analyzed in this paper.

To understand the biases in modeling dust and its direct radiative forcing over the East Asia, a variety of in situ measurements and satellite retrievals are used to evaluate the simulations over and near the major dust source regions. Overall, WRF-Chem model reasonably reproduces the temporal variations of observed aerosol optical properties (AOD, extinction profiles, and SSA) and size

distributions near the dust source regions during the simulation period. We can found the model generally captures the MISR retrieved seasonal aerosol optical depth (AOD) variations over the Taklimakan Desert (TD) and Gobi Desert (GD), indicating the model is capable of simulating the overall characteristics of mineral dust over the large regions of the dust source region. However, the model has a positive bias in dust AOD in summer and fall compared to MISR retrievals. The bias seems not from the errors in the simulated seasonal variations of 10-m surface winds that are generally consistent with the observations. This bias in seasonal variations of dust AOD above the TD and GD needs further investigation. In

Table 2
Summary of dust direct radiative forcing over East Asia in previous studies.

TOA (W/m²)	ATM (W/m²)	BOT (W/m²)	Region	Time	Method	References
−3 (SW)		−17 (SW)	100°E–150°E; 20°N–50°N	April 5–15 2001	CFORS model [a]	Conant et al. (2003)
−2.9	3.8	−6.8	East Asia	March 2002	Asian Dust Aersol Model	Park and Jeong (2008)
−5	–	−15	East Asian deserts	[b]FMAM 1997–2006	[c]RegCM3	Zhang et al. (2009)
0.94	–	−3.93	75–145°E, 15–55°N	19–22 March 2010	[d]RIEMS-Chemaero	Han et al. (2011)
1.18	–	−8.42	East China			
1.40	–	−6.09	West China			
−13.6 (SW)	23.2 (SW)	−36.8 (SW)	The Yangtze Delta region of China	March 14–17 and April 25–26 2009	SBDART model[e]	Liu et al. (2011)
5.93–35.7	16.77–56.32	−6.3 to −30.94	[f]Minqin, SACOL	April 24–30 2010	Fu-Liou radiative transfer model	Wang et al. (2013)
Up to −8 (SW) Up to 2 (LW)	–	Up to −25 (SW) Up to 8 (LW)	East Asian deserts	Spring and summer of 2000–2009	[g]RegCM4	Sun et al. (2012)
−3.97	1.61	−5.58	TP	26–30 July 2006	WRF-Chem	Chen et al. (2013)

[a] A three-dimensional atmospheric chemical transport model (Chemical Weather Forecast System (CFORS)).
[b] February–March–April–May (FMAM).
[c] Regional Climate Model Version 3 (RegCM3).
[d] RIEMS-Chemaero represents an online-coupled regional climate-chemistry-aerosol model.
[e] The Santa Barbara DISORT Atmospheric Radiative Transfer model (SBDART model).
[f] Minqin (36.61°N, 102.96°E) is located in a semi-desert area of northwest China.
[g] Regional Climate Model Version 4 (RegCM4).

addition, model bias is also identified for simulating aerosol SSA near the dust source regions. This is likely due to that the observation site is also frequently affected by the local pollutions (e.g., black carbon) that cannot be fully represented by the WRF-Chem simulations. The observations over the dust source regions isolated from the anthropogenic impact are needed in order to better evaluate the simulated dust optical properties. In terms of size distribution, the simulation captures the seasonal variations of the observed size distributions but overestimates the fine and underestimates the coarse dust particles. This has been found to be the bias from the mode size representation and can be improved with a more accurate dust size representation (e.g., 8-size bin) (Zhao et al., 2013a). Nevertheless, it should also be noted that some uncertainties also exist in observations. For example, at the SACOL site, the MPL retrieved AOD is less than that from AERONET in winter due to the uncertainty of lidar ratio during retrieving.

The dust mass balance and its contributions from various sources and sinks are analyzed for seven selected sub-regions of East Asia (TD, GD, TP, Northern China, Southern China, the ocean outflow region, and Korea-Japan). TD and GD are two dominant dust source regions over East Asia. Over both regions, dry deposition and transport processes are the two major sinks of dust. Transport contribution to the dust sink is larger over the GD (36%) than TD (25%), partly due to the complex terrain of TD basin that does not favor dust transport. This is consistent with previous studies (Sun et al., 2001; Zhang et al., 2008) that found the GD dust has a larger impact at regional scale than the TD dust. Over the TP, the dust column mass concentration reaches a maximum in summer because of dust transport from the TD, which is consistent with the case study analyzed by Chen et al. (2013). Over other regions, dust column mass concentration is mainly contributed by transport and reaches maximum in spring. In these high-polluted regions with large amount of anthropogenic aerosols, the dust contribution to the total aerosol loading is relatively small. Dry and wet depositions are the comparable dominant sinks over most of these regions, except for Korea–Japan where wet deposition contribution (70%) is larger than dry deposition contribution (30%), particularly in spring.

Generally, dust direct radiative forcing results in atmospheric warming, surface cooling, and TOA cooling over East Asia. The net (SW + LW) dust direct radiative forcing at the TOA has a cooling effect of −4 W m⁻² on domain average with a maximum of −8 W m⁻². In the atmosphere, dust produces a net warming effect with a domain average of 3 W m⁻² and a maximum of 20 W m⁻². At the surface, dust results in a cooling effect of −7 W m⁻² on domain average. The dust direct radiative forcing averaged over the seven sub-regions of East Asia is summarized in Table 1. Some of previous modeling estimates of dust direct radiative forcing over East Asia are also summarized in Table 2. It shows that our estimates of dust direct radiative forcing over East Asia are generally comparable with previous modeling studies (Park and Jeong, 2008; Zhang et al., 2009; Han et al., 2012; Wang et al., 2012; Sun et al., 2012; Chen et al., 2013). It should be noted that some previous studies listed in the table cannot be directly compared since they only estimated dust SW radiative forcing. In addition, this study first time estimates the dust direct radiative forcing over different regions of East Asia and provides annual and seasonal mean values, compared to previous studies that merely provided the average dust direct radiative forcing for a season (e.g., spring) or even shorter at one site or over the source regions only. Furthermore, dust direct radiative forcing depends on dust column concentration, size distributions, and optical properties (e.g., SSA). This makes difficult to compare our estimates directly with previous estimates. For example, Zhang et al. (2009) and Sun et al. (2012) used similar models to estimate dust direct radiative forcing over the source regions in spring. They obtained close values of dust cooling effect of about −15 W m⁻² at the surface and −5 W m⁻² at the TOA. Our estimates of dust direct radiative forcing over the TD and GD in spring are about −10 W m⁻² at the surface and −5 W m⁻² at the TOA. Although we are consistent in estimating dust TOA cooling, our estimated dust surface cooling is less than theirs. This difference resulted from the model difference in estimating dust absorption in the atmosphere, which could be due to the difference in prescribing dust absorptivity and simulating dust size distribution.

The major deserts of TD and GD emit dust that has far reaching influence through transport of dust that perturbs atmospheric energy. Climate change can potentially strengthen subtropical drying, leading to increased dust emission in our study regions. This study highlights the importance of including dust radiative feedbacks in understanding large-scale and regional climate variations and changes over East Asia. Interactions of dust with clouds and precipitation have not been a focus of this study, but dust also has

potentially large effects on precipitation amount and phase (Zhao et al., 2011, 2012; Creamean et al., 2013; Fan et al., 2013), and these effects over East Asia need further investigation in future studies.

Acknowledgements

References

Ackermann, I.J., Hass, H., Memmesheimer, M., Ebel, A., Binkowski, F.S., Shankar, U., 1998. Modal aerosol dynamics model for Europe: development and first applications. Atmos. Environ. 32, 2981–2999. Available from: <http://dx.doi.org/10.1016/S1352-2310(98)00006-5>.

Balkanski, Y., Schulz, M., Claquin, T., Guibert, S., 2007. Reevaluation of Mineral aerosol radiative forcings suggests a better agreement with satellite and AERONET data. Atmos. Chem. Phys. 7, 81–95. http://dx.doi.org/10.5194/acp-7-81-2007.

Barnard, J.C., Fast, J.D., Paredes-Miranda, G., Arnott, W.P., Laskin, A., 2010. Technical note: evaluation of the WRF-Chem aerosol chemical to aerosol optical properties module using data from the MILAGRO campaign. Atmos. Chem. Phys. 10, 7325–7340. http://dx.doi.org/10.5194/acp-10-7325-2010.

Bennartz, R., Fan, J., Rausch, J., Leung, L.R., Heidinger, A.K., 2011. Pollution from China increases cloud droplet number, suppresses rain over the East China Sea. Geophys. Res. Lett. 38, L09704. http://dx.doi.org/10.1029/2011GL047235.

Bi, J.R., Huang, J., Fu, Q., Wang, X., Shi, J., Zhang, W., Huang, Z., Zhang, B., 2011. Toward characterization of the aerosol optical properties over Loess Plateau of Northwestern China. J. Quantum Spectrosc. Ra. 112, 346–360. http://dx.doi.org/10.1016/j.jqsrt.2010.09.006.

Chen, F., Dudhia, J., 2001. Coupling an advanced land surface-hydrology model with the Penn State-NCAR MM5 modeling system. Part I: model implementation and sensitivity. Mon. Weather Rev. 129, 569–585, http://dx.doi.org/10.1175/1520-0493(2001) 129<0569:CAALSH>2.0.CO;2.

Chen, F., Mitchell, K., Schaake, J., Xue, Y., Pan, H.-L., Koren, V., Duan, Q.Y., Ek, M., Betts, A., 1996. Modeling of land surface evaporation by four schemes and comparison with FIFE observations. J. Geophys. Res. 101 (D3), 7251–7268. http://dx.doi.org/10.1029/95JD02165.

Chen, Y.S., Sheen, P.C., Chen, E.R., Liu, Y.K., Wu, T.N., Yang, C.Y., 2004. Effects of Asian dust storm events on daily mortality in Taipei∗ Taiwan. Environ. Res. 95, 151–155, doi: 10.1016/j.envres.2003.08.008, 2004.

Chen, S., Huang, J., Zhao, C., Qian, Y., Leung, L.R., Yang, B., 2013. Modeling the transport and radiative forcing of Taklimakan dust over the Tibetan Plateau: a case study in the summer of 2006. J. Geophys. Res. Atmos. 118, 797–812. http://dx.doi.org/10.1002/jgrd.50122.

Claquin, T. et al., 1998. Uncertainties in assessing radiative forcing by mineral dust. Tellus Ser. B 50 (5), 491–505. http://dx.doi.org/10.1034/j.1600-0889.1998.t01-2-00007.x.

Creamean, J.M. et al., 2013. Dust and biological aerosols from the Sahara and Asia influence precipitation in the western US, Science. DOI: 10.1126/science.1227279.

DeMott, P.J., Prenni, A., Liu, X., et al., 2010. Predicting global atmospheric ice nuclei distributions and their impacts on climate. Proc. Natl. Acad. Sci. USA 107, 11217–11222. http://dx.doi.org/10.1073/pnas.0910818107.

Dubovik, O., King, M.D., 2000. A fexible inversion algorithm for retrieval of aerosol optical properties from sun and sky radiance measurements. J. Geophys. Res. 105, 20673–20696. http://dx.doi.org/10.1029/2000JD900282.

Dubovik, O., Holben, B., Eck, T.F., Smirnov, A., et al., 2002. Variability of absorption and optical properties of key aerosol types observed in worldwide locations. J. Atmos. Sci. 59, 590–608, http://dx.doi.org/10.1175/1520-0469(2002) 059<0590:VOAAOP>2.0.CO;2.

Fan, J., Leung, L.R., DeMott, P., Comstock, J., Singh, B., Rosenfeld, D., Tomlinson, JM., White, A., Prather, KA., Minnis, P., Ayers, JK., Min Q., 2013. Aerosol impacts on California winter clouds and precipitation during CalWater 2011: local pollution versus long-range transported dust. Atmos. Chem. Phys. (in review).

Fast, J.D., Gustafson Jr., W.I., Easter, R.C., Zaveri, R.A., Barnard, J.C., Chapman, E.G., Grell, G.A., Peckham, S.E., 2006. Evolution of ozone, particulates, and aerosol direct radiative forcing in the vicinity of Houston using a fully coupled meteorology-chemistry-aerosol model. J. Geophys. Res. 111, D21305. http://dx.doi.org/10.1029/2005JD006721.

Fernald, F.G., 1984. Analysis of atmospheric lidar observations: Some comments. Appl. Opt. 23, 652–653.

Ge, J., Su, J., Fu, Q., Ackerman, T.P., Huang, J., 2010a. Dust aerosol forward scattering effects on ground-based aerosol optical depth retrievals. J. Quant. Spectrosc. Radiat. Transfer 112. http://dx.doi.org/10.1016/j.jqsrt.2010.07.006.

Ge, J., Su, J. Ackerman, T.P., Fu, Q., Huang, J., Shi, J., 2010. Dust aerosol optical properties retrieval and radiative forcing over northwestern China during the 2008 China–US joint field experiment, J. Geophys. Res. 115, D00K12. doi: 10.1029/1009JD013263.

Ge, J., Huang, J., Su, J., Bi, J., Fu, Q., 2011. Shortwave radiative closure experiment and direct forcing of dust aerosol over northwestern China. Geophys. Res. Lett. 38, L24803. http://dx.doi.org/10.1029/2011GL049571.

Ginoux, P., Chin, M., Tegen, I., Prospero, J.M., Holben, B., Dubovik, O., Lin, S., 2001. Sources and distributions of dust aerosols simulated with the GOCART model. J. Geophys. Res. 106 (D17), 20225–20273. http://dx.doi.org/10.1029/2000JD000053.

Gong, S.L., Zhang, X.Y., Zhao, T.L., McKendry, I.G., Jaffe, D.A., Lu, N.M., 2003. Characterization of soil dust aerosol in China and its transport and distribution during 2001 ACE-Asia: 2. Model simulation and validation. J. Geophys. Res. 108 (D9), 4262. http://dx.doi.org/10.1029/2002JD002633.

Grell, G.A., Peckham, S.E., Schmitz, R., McKeen, S.A., Frost, G., Skamarock, W.C., Eder, B., 2005. Fully coupled online chemistry within the WRF model. Atmos. Environ. 39, 6957–6976.

Han, Z., Li, J., Xia, X., Zhang, R., 2012. Investigation of direct radiative effects of aerosols in dust storm season over East Asia with an online coupled regional climate-chemistry-aerosol model. Atmos. Environ. 54, 688–699.

Hanna, S.R., Yang, R., Yin, X., 2000. Evaluations of numerical weather prediction (NWP) models from the point of view of inputs required by atmospheric dispersion models. Int. J. Environ. Pollut. 14 (1–6), 98–105. http://dx.doi.org/10.1504/IJEP.2000.000530.

Hess, M., Koepke, P., Schult, I., 1998. Optical properties of aerosols and clouds: the software package OPAC. Bull. Am. Meteorol. Soc. 79, 831–844, http://dx.doi.org/10.1175/1520-0477(1998) 079<0831:OPOAAC>2.0.CO;2.

Holben, B.N. et al., 1998. AERONET-a federated instrument network and data archive for aerosol characterization. Remote Sensing Environ 66, 1–16. http://dx.doi.org/10.1016/S0034-4257(98)00031-5.

Hong, S.Y., Noh, Y., Dudhia, J., 2006. A new vertical diffusion package with an explicit treatment of entrainment processes. Mon. Weather Rev. 134, 2318–2341, http://dx.doi.org/10.1175/MWR3199.1.

Huang, J., Minnis, P., Lin, B., Wang, T., Yi, Y., Hu, Y., Sun-Mack, S., Ayers, K., 2006a. Possible influences of Asian dust aerosols on cloud properties and radiative forcing observed from MODIS and CERES. Geophys. Res. Lett. 33, L06824. http://dx.doi.org/10.1029/2005GL024724.

Huang, J., Lin, B., Minnis, P., Wang, T., Wang, X., Hu, Y., Yi, Y., Ayers, J.K., 2006b. Satellite-based assessment of possible dust aerosols semi-direct effect on cloud water path over East Asia. Geophys. Res. Lett. 33, L19802. http://dx.doi.org/10.1029/2006GL026561.

Huang, J., Minnis, P., Yi, Y., Tang, Q., Wang, X., Hu, Y., Liu, Z., Ayers, K., Trepte, C., Winker, D., 2007. Summer dust aerosols detected from CALIPSO over the Tibetan Plateau. Geophys. Res. Lett. 34 (L18805), 2007. http://dx.doi.org/10.1029/2007GL029938.

Huang, J., Minnis, P., Chen, B., Huang, Z., Liu, Z., Zhao, Q., Yi, Y., Ayers, J.K., 2008a. Long-range transport and vertical structure of Asian dust from CALIPSO and surface measurements during PACDEX. J. Geophys. Res. 113, D23212. http://dx.doi.org/10.1029/2008JD010620.

Huang, J. et al., 2008b. An overview of the Semi-Arid climate and environment research observatory over the loess plateau. Adv. Atmos. Sci. 25 (6), 906–921. http://dx.doi.org/10.1007/s00376-008-0906-7.

Huang, J., Fu, Q., Su, J., Tang, Q., Minnis, P., Hu, Y., Yi, Y., Zhao, Q., 2009. Taklimakan dust aerosol radiative heating derived from CALIPSO observations using the Fu-Liou radiation model with CERES constraints. Atmos. Chem. Phys. 9, 4011–4021. http://dx.doi.org/10.5194/acp-9-4011-2009.

Huang, Z., Sugimoto, N., Huang, J., Hayasaka, T., Nishizawa, T., Bi, J., Matsui, I., 2010. Comparison of depolarization ratio measurements with Micro-pulse Lidar and a linear polarization lidar in Lanzhou, China. In: Proc. of 25th International Laser Radar Conference, 1, pp. 528–531.

Huang, J., Fu, Q., Zhang, W., Wang, X., Zhang, R., Ye, H., Warren, S., 2011. Dust and black carbon in seasonal snow Across Northern China. Bull. Am. Meteorol. Soc. 92, 175–181. http://dx.doi.org/10.1175/2010BAMS3064.1.

Iacono, M.J., Mlawer, E.J., Clough, S.A., Morcrette, J.J., 2000. Impact of an improved longwave radiation model, RRTM, on the energy budget and thermodynamic properties of the NCAR community climate model, CCM3. J. Geophys. Res. 105, 14. http://dx.doi.org/10.1029/2000JD900091.

Jiménez, Pedro.A., Dudhia, Jimy., 2012. Improving the representation of resolved and unresolved topographic effects on surface wind in the WRF model. J. Appl. Meteorol. Climatol. 51, 300–316, http://dx.doi.org/10.1175/JAMC-D-11-084.1.

Kain, John S., 2004. The Kain–Fritsch convective parameterization: an update. J. Appl. Meteorol. 43, 170–181, http://dx.doi.org/10.1175/1520-0450(2004) 043<0170:TKCPAU>2.0.CO;2.

Kain, John S., Michael Fritsch, J., 1990. A one-dimensional entraining/detraining plume model and its application in convective parameterization. J. Atmos. Sci. 47, 2784–2802, http://dx.doi.org/10.1175/1520-0469(1990) 047<2784:AODEPM>2.0.CO;2.

Kalenderski, S., Stenchikov, G., Zhao, C., 2013. Modeling a typical winter-time dust event over the Arabian Peninsula and the Red Sea. Atmos. Chem. Phys. 13, 1999–2014. http://dx.doi.org/10.5194/acp-13-1999-2013.

Kim, K.W., Kim, Y.J., Oh, S.J., 2001. Visibility impairment during Yellow Sand periods in the urban atmosphere of Kwangju, Korea. Atmos. Environ. 35 (30), 5157–5167.

Krinner, G., Boucher, O., Balkanski, Y., 2006. Ice-free glacial northern Asia due to dust deposition on snow. Clim. Dyn. 27, 613–625.

Liu, Z., Liu, D., Huang, J., Vaughan, M., Uno, I., Sugimoto, N., Kittaka, C., Trepte, C., Wang, Z., Hostetler, C., Winker, D., 2008. Airborne dust distributions over the Tibetan Plateau and surrounding areas derived from the first year of CALIPSO lidar observations. Atmos. Chem. Phys. 8, 5957–5977. http://dx.doi.org/10.5194/acp-8-5045-200.

Liu, Y., Huang, J., Shi, G., Takamura, T., Khatri, P., Bi, J., Shi, J., Wang, T., Wang, X., Zhang, B., 2011. Aerosol optical properties and radiative effect determined from sky-radiometer over Loess Plateau of Northwest China. Atmos. Chem. Phys. 11, 11455–11463.

Mahowald, N., Engelstaedter, S., Luo, C., Sealy, A., Artaxo, P., Benitez-Nelson, C., Bonnet, S., Chen, Y., Chuang, P.Y., Cohen, D.D., Dulac, F., Herut, B., Johansen, A.M., Kubilay, N., Losno, R., Maenhaut, W., Paytan, A., Prospero, J.M., Shank, L.M., Siefert, R.L., 2009. Atmospheric Iron deposition: Global distribution, variability and human perturbations. Annu. Rev. Mar. Sci. 1, 245–278. http://dx.doi.org/10.1146/annurev.marine.010908.163727.

Martonchik, J.V., Diner, D.J., Kahn, R.A., Ackerman, T.P., Verstraete, M.M., Pinty, B., Gordon, H.R., 1998. Techniques for the retrieval of aerosol properties over land and ocean using multiangle imaging. IEEE Trans. Geosci. Remote Sens. 36, 1212–1227, http://dx.doi.org/10.1109/36.701027.

Martonchik, J.V., Diner, D.J., Crean, K.A., Bull, M.A., 2002. Regional aerosol retrieval results from MISR. IEEE Trans. Geosci. Remote Sens. 40, 1520–1531. http://dx.doi.org/10.1109/TGRS.2002.801142.

Martonchik, J., Diner, D., Kahn, R., Gaitley, B., Holben, B., 2004. Comparison of MISR and AERONET aerosol optical depths over desert sites. Geophys. Res. Lett. 31, L16102. http://dx.doi.org/10.1029/2004GL019807.

Mass, C., Ovens, D., 2011. Fixing WRF's high speed wind bias: A new subgrid scale drag parameterization and the role of detailed verification. In: Preprints, 24th Conf. on Weather and Forecasting/20th Conf. on Numerical Weather Prediction, Seattle, WA, Amer. Meteor. Soc., 9B.6. Available online at: http://ams.confex.com/ams/91Annual/webprogram/Paper180011.html.

McKeen, S.A., Wotawa, G., Parrish, D.D., Holloway, J.S., Buhr, M.P., Hübler, G., Fehsenfeld, F.C., Meagher, J.F., 2002. Ozone production from Canadian wildfires during June and July of 1995, J. Geophys. Res. 107, 4192. doi:10.1029/2001JD000697.

Mlawer, E.J., Taubman, S.J., Brown, P.D., Iacono, M.J., Clough, S.A., 1997. RRTM, a validated correlated-k model for the longwave. J. Geophys. Res. 102, 16663–16682. http://dx.doi.org/10.1029/97JD00237.

Morrison, H., Curry, J., Khvorostyanov, V., 2005. A new doublemoment microphysics parameterization for application in cloud and climate models. Part I: description. J. Atmos. Sci. 62, 1665–1677, http://dx.doi.org/10.1175/JAS3446.1.

Osborne, S.R., Johnson, B.T., Haywood, J.M., Baran, A.J., Harrison, A.J., McConnell, C.L., 2008. Physical and optical properties of mineral dust aerosol during the Dust and Biomass-burning Experiment, J. Geophys. Res. 113, D00C03. doi:10.1029/2007JD009551.

Painter, T.H., Deems, J.S., Belnap, J., Hamlet, A.F., Landry, C.C., Udall, B., 2010. Response of Colorado River runoff to dust radiative forcing in snow. Proc. Nat. Acad. Sci. 107 (40), 17125–17130. http://dx.doi.org/10.1073/pnas.0913139107.

Painter, T.H., Skiles, S.M., Deems, J.M., Bryant, A.C., Landry, C.C., 2012. Dust radiative forcing in snow of the Upper Colorado River Basin: 1. A 6 year record of energy balance, radiation, and dust concentrations. Water Resour. Res. 48, W07521. doi:10.1029/2012WR011985.

Park, S.-U., Jeong, J.I., 2008. Direct radiative forcing due to aerosols in Asia during March 2002. Sci. Total Environ. 407, 394–404.

Petrenko, M., Ichoku, C., 2013. Coherent uncertainty analysis of aerosol measurements from multiple satellite sensors. Atmos. Chem. Phys. 13, 6777–6805.

Qian, Y., Flanner, M., Leung, L.R., Wang, W., 2011. Sensitivity studies on the impacts of Tibetan Plateau snowpack pollution on the Asian hydrological cycle and monsoon climate. Atmos. Chem. Phys. 11, 1929–1948. http://dx.doi.org/10.5194/acp-11-1929-2011.

Rea, D.K., 1994. The paleoclimatic record provided by eolian deposition in the deep sea: the geologic history of wind. Rev. Geophys. 32 (2), 159–195. http://dx.doi.org/10.1029/93RG03257.

Schell, B., Ackermann, I.J., Hass, H., Binkowski, F.S., Ebel, A., 2001. Modeling the formation of secondary organic aerosol within a comprehensive air quality modeling system. J. Geophys. Res. 106, 28275–28293. http://dx.doi.org/10.1029/2001JD000384.

Shao, Y., Wang, W.J., 2003. A climatology of Northeast Asian dust events, Meteorologische Zeitschrift, Volume 12, Number 4, 1 August 2003, pp. 187–196(10). doi: http://dx.doi.org/10.1127/0941-2948/2003/0012-0187.

Shao, Y., Klose, M., Wyrwoll, K.-H., 2013. Recent global dust trend and connections to climate forcing. J. Geophys. Res. Atmos. 118, 11,107–11,118. doi: 10.1002/jgrd.50836.

Skamarock, W.C., Klemp, J.B., Dudhia, J., Gill, D.O., Barker, D.M., Duda, M.G., Huang, X., Wang, W., Powers, J.G., 2008. A description of the advanced research WRF version 3, NCAR Tech. Note, NCAR/TN-475+STR, 8 pp., Natl. Cent. for Atmos. Res., Boulder, CO, USA. Available at: <http://www.mmm.ucar.edu/wrf/users/docs/arw v3.pdf>.

Skiles, S.M., Painter, T.H., Deems, J.M., Bryant, A.C., Landry, C.C., 2012. Dust radiative forcing in snow of the Upper Colorado River Basin: 2. Interannual variability in radiative forcing and snowmelt rates. Water Resour. Res. 48, W07522. http://dx.doi.org/10.1029/2012WR011986.

Sokolik, I.N., Winker, D.M., Bergametti, G., Gillette, D.A., Carmichael, G., Kaufman, Y.J., Gomes, L., Schuetz, L., Penner, J.E., 2001. Introduction to special section: outstanding problems in quantifying the radiative impacts of mineral dust, J. Geophys. Res. 106, 18,015–18,027.

Spinhirne, J.D., 1993. Micro Pulse Lidar. IEEE Trans. Geosci. Remote Sens. 31, 48–55. http://dx.doi.org/10.1109/36.210443.

Stauffer, D.R., Seaman, N.L., 1990. Use of four-dimensional data assimilation in a limited-area mesoscale model. Part I: experiments with synoptic-scale data. Mon. Weather Rev. 118, 1250–1277, http://dx.doi.org/10.1175/1520-0493(1990) 118<1250:UOFDDA>2.0.CO;2.

Sun, J., Zhang, M., Liu, T., 2001. Spatial and temporal characteristics of dust storms in China and its surrounding regions, 1960–1999: relations to source area and climate. J. Geophys. Res. 106 (D10), 10325–10333. http://dx.doi.org/10.1029/2000JD900665.

Sun, H., Pan, Z., Liu, X., 2012. Numerical simulation of spatial-temporal distribution of dust aerosol and its direct radiative effects on East Asian climate. J. Geophys. Res. 117 (D13206), 2012.

Thomson, M.C., Molesworth, A.M., Djingarey, M.H., Yameogo, K.R., Belanger, F., Cuevas, L.E., 2006. Potential of environmental models to predict meningitis epidemics in Africa. Trop. Med. Int. Health 11 (6), 781–788. http://dx.doi.org/10.1111/j.1365-3156.2006.01630.x.

Uno, I., Eguchi, K., Yumimoto, K., Takemura, T., Shimizu, A., Uematsu, M., Liu, Z., Wang, Z., Hara, Y., Sugimoto, N., 2009. Asian dust transported one full circuit around the globe. Nat. Geosci. 2, 557–560. http://dx.doi.org/10.1038/ngeo583.

van der Werf, G.R., Randerson, J.T., Giglio, L., Collatz, G.J., Mu, M., Kasibhatla, P.S., Morton, D.C., DeFries, R.S., Jin, Y., van Leeuwen, T.T., 2010. Global fire emissions and the contribution of deforestation, savanna, forest, agricultural, and peat fires (1997–2009). Atmos. Chem. Phys. 10, 11707–11735. http://dx.doi.org/10.5194/acpd-10-16153-2010.

Wang, X., Huang, J., Ji, M., Higuchi, K., 2008. Variability of East Asia dust events and their long-term trend. Atmos. Environ. 42, 3156–3165. http://dx.doi.org/10.1016/j.atmosenv.2007.04.046.

Wang X., Huang J., Zhang R., Chen, B., Bi, J., 2010. Surface measurements of aerosol properties over northwest China during ARM China 2008 deployment, J. Geophys. Res. 115, D00K27. doi:10.1029/2009JD013467.

Wang, K., Zhang, Y., Nenes, A., Fountoukis, C., 2012. Implementation of dust emission and chemistry into the Community Multiscale Air Quality modeling system and initial application to an Asian dust storm episode. Atmos. Chem. Phys. 12, 10209–10237.

Wang, W., Huang, J., Zhou, T., Bi, J., Lin, L., Chen, Y., Huang, Z., Su, J., 2013. Estimation of radiative effect of a heavy dust storm over northwest China using Fu–Liou model and ground measurements. J. Quant. Spectrosc. Radiat. Transfer 122, 114–126.

Welton, E.J., Campbell, J.R., Spinhirne, J.D., Scott, V.S., 2001. Global monitoring of clouds and aerosols using a network of micropulse lidar systems. Proc. SPIE Int. Soc. Opt. Eng. 4153, 151–158. http://dx.doi.org/10.1117/12.417040.

Zhang, X.Y., Arimoto, R., An, Z.S., 1997. Dust emission from Chinese desert sources linked to variations in atmospheric circulation, J. Geophys. Res. 102(D23), 28,041–28,044. doi:10.1029/97JD02300.

Zhang, X.Y., Gong, S.L., Zhao, T.L., Arimoto, R., Wang, Y.Q., Zhou, Z.J., 2003. Sources of Asian dust and role of climate change versus desertification in Asian dust emission. Geophys. Res. Lett. 30 (24), 2272. http://dx.doi.org/10.1029/2003GL018206.

Zhang, B., Tsunekawa, A., Tsubo, M., 2008. Contributions of sandy lands and stony deserts to long-distance dust emission in China and Mongolia during 2000–2006. Global Planet. Change 60 (3–4), 487–504. http://dx.doi.org/10.1016/j.gloplacha.2007.06.001.

Zhang, D.F., Zakey, A.S., Gao, X.J., Giorgi, F., Solmon, F., 2009. Simulation of dust aerosol and its regional feedbacks over East Asia using a regional climate model. Atmos. Chem. Phys. 9, 1095–1110.

Zhao, C., Liu, X., Leung, L.R., Johnson, B., McFarlane, S., Gustafson Jr., W., Fast, J., Easter, R., 2010. The spatial distribution of mineral dust and its shortwave radiative forcing over North Africa: modeling sensitivities to dust emissions and aerosol size treatments. Atmos. Chem. Phys. 10, 8821–8838. http://dx.doi.org/10.5194/acp-10-8821-2010.

Zhao, C., Liu, X., Leung, L.R., Hagos, S., 2011. Radiative impact of mineral dust on monsoon precipitation variability over West Africa. Atmos. Chem. Phys. 11, 1879–1893. http://dx.doi.org/10.5194/acp-11-1879-2011.

Zhao, C., Liu, X., Leung, L.R., 2012. Impact of the Desert dust on the summer monsoon system over Southwestern North America. Atmos. Chem. Phys. 12, 3717–3731. http://dx.doi.org/10.5194/acp-12-3717-2012.

Zhao, C., Chen, S., Leung, LR., Qian, Y., Kok, J., Zaveri, R., Huang, J., 2013a. Uncertainty in modeling dust mass balance and radiative forcing from size parameterization. Atmos. Chem. Phys.

Zhao, C., Ruby Leung, L., Easter, R., Hand, J., Avise, J., 2013b. Characterization of speciated aerosol direct radiative forcing over California. J. Geophys. Res. Atmos. 118, 2372–2388. http://dx.doi.org/10.1029/2012JD018364.

Zhou, B., Zhang, L., Cao, X., Li, X., Huang, J., Shi, J., Bi, J., 2012. Analysis of the vertical structure and size distribution of dust aerosols over the semi-arid region of the Loess Plateau in China. Atmos. Chem. Phys. Discuss. 12, 6113–6143. 2012.www.atmos-chem-phys-discuss.net/12/6113/2012/doi:10.5194/acpd-12-6113-2012.

Zhou, T., Huang, J.P., Huang, Z.W., Liu, J.J., Wang, W.C., Lin, L., 2013. The depolarization-attenuated backscatter relationship for dust plumes. Opt. Express 13 (21), 15195–15204. http://dx.doi.org/10.1364/OE.21.015195.